nature immunology

ARTICLES

https://doi.org/10.1038/s41590-018-0083-5

Corrected: Publisher Correction

c-Maf controls immune responses by regulating disease-specific gene networks and repressing IL-2 in CD4+ T cells

Leona Gabryšová[1], Marisol Alvarez-Martinez[1], Raphaëlle Luisier[2], Luke S. Cox[1], Jan Sodenkamp[3], Caroline Hosking[3], Damián Pérez-Mazliah[3], Charlotte Whicher[1], Yashaswini Kannan[4], Krzysztof Potempa[1], Xuemei Wu[1], Leena Bhaw[5], Hagen Wende[6], Michael H. Sieweke[7,8], Greg Elgar[5], Mark Wilson[4], James Briscoe[9], Vicki Metzis[9], Jean Langhorne[3], Nicholas M. Luscombe[2,10] and Anne O'Garra[1,11]*

The transcription factor c-Maf induces the anti-inflammatory cytokine IL-10 in CD4+ T cells in vitro. However, the global effects of c-Maf on diverse immune responses in vivo are unknown. Here we found that c-Maf regulated IL-10 production in CD4+ T cells in disease models involving the T_H1 subset of helper T cells (malaria), T_H2 cells (allergy) and T_H17 cells (autoimmunity) in vivo. Although mice with c-Maf deficiency targeted to T cells showed greater pathology in T_H1 and T_H2 responses, T_H17 cell–mediated pathology was reduced in this context, with an accompanying decrease in T_H17 cells and increase in Foxp3+ regulatory T cells. Bivariate genomic footprinting elucidated the c-Maf transcription-factor network, including enhanced activity of NFAT; this led to the identification and validation of c-Maf as a negative regulator of IL-2. The decreased expression of the gene encoding the transcription factor RORγt (*Rorc*) that resulted from c-Maf deficiency was dependent on IL-2, which explained the in vivo observations. Thus, c-Maf is a positive and negative regulator of the expression of cytokine-encoding genes, with context-specific effects that allow each immune response to occur in a controlled yet effective manner.

The immune response is under strict control in its regulation of the production of inflammatory mediators that control infection with minimal damage to the host. Subsets of CD4+ helper T cells, including T_H1, T_H2 and T_H17 cells, are critical for the eradication of specific pathogens[1], but if they are uncontrolled, they can contribute to immunopathology, either during infection or during immune system–mediated diseases[2,3]. Various regulatory mechanisms are in place to control inappropriate or excessive immune responses, including production of the anti-inflammatory cytokine IL-10[4] and CD4+ regulatory T cells (T_{reg} cells) expressing the gene encoding the transcription factor (TF) Foxp3[5]. Although distinct molecular pathways direct the development of different effector and regulatory CD4+ T cells, IL-10 is produced by all CD4+ T cell subsets and is therefore not a subset-specific cytokine[4]. Whether IL-10 production is regulated by lineage-specific mechanisms or whether a common TF controls IL-10 in all CD4+ T cell subsets is unclear. Many TFs[6–20] have been shown to modulate *Il10* expression, including c-Maf, a member of the AP-1 ('activator protein-1') TF superfamily[7,16,19–21]. c-Maf functions to control an array of biological processes, including lens and bone development, apoptosis, oncogenesis and the immune response[22]. Although c-Maf has been shown to positively regulate *Il10* expression in vitro[6,7,16,21], its effects on *Il10* and global gene expression across different immune responses in vivo are unknown.

Here we found that c-Maf regulated IL-10 in vivo in CD4+ T cells from disease models involving T_H1 cells (malaria), T_H2 cells (allergy) and T_H17 cells (autoimmunity) but had context-specific effects on these immune responses beyond its effects on IL-10. Through the use of genomic approaches, we found that c-Maf-deficient CD4+ T cells showed substantial changes in transcriptional activity, including enhanced activity of the TF NFAT, which led to the identification and validation of c-Maf as a negative regulator of IL-2. This provided an explanation for the context-specific effects of c-Maf deficiency on the immune responses, which included decreased T_H17 cells, increased Foxp3+ T_{reg} cells and reduced autoimmune pathology in vivo.

Results

Expression of *Maf* and that of *Il10* correlate in all helper T cell and T_{reg} cell subsets. To identify candidate TFs that regulate the expression of *Il10* in different CD4+ T cell subsets, we differentiated T_H1, T_H2, T_H17 and T cells in vitro and profiled the following cells by RNA-based next-generation sequencing (RNA-seq): T_H1 cells, T_H1 cells grown in the presence of IL-27[23], T_H2 cells, T_H17 cells, and T cells that produce IL-10 only and were grown in the presence of vitamin D_3 and dexamethasone[24], as well as ex vivo–derived Foxp3+ T_{reg} cells (Fig. 1a–d). We correlated the expression of

[1]The Francis Crick Institute, Laboratory of Immunoregulation and Infection, London, UK. [2]The Francis Crick Institute, Computational Biology Laboratory, London, UK. [3]The Francis Crick Institute, Malaria Laboratory, London, UK. [4]The Francis Crick Institute, Helminth Immunology Laboratory, London, UK. [5]The Francis Crick Institute, Advanced Sequencing Facility Laboratory, London, UK. [6]Heidelberg University, Institute of Pharmacology, Heidelberg, Germany. [7]Aix Marseille University, CNRS, INSERM, CIML, Marseille, France. [8]Max-Delbrück-Centrum für Molekulare Medizin in der Helmholtzgemeinschaft (MDC), Berlin, Germany. [9]The Francis Crick Institute, Developmental Dynamics Laboratory, London, UK. [10]UCL Genetics Institute, Department of Genetics, Evolution and Environment, University College London, London, UK. [11]National Heart and Lung Institute, Imperial College London, London, UK. *e-mail: anne.ogarra@crick.ac.uk

TF-encoding genes to that of *Il10* mRNA across all helper T cell and T_{reg} cell subsets (Fig. 1e and Supplementary Table 1). c-Maf, which is encoded by a gene (*Maf*) that was upregulated upon differentiation (Supplementary Fig. 1), was the strongest candidate as a positive regulator of *Il10* (Fig. 1e,f) among TFs previously associated with IL-10[6–17,21,25] (Fig. 1e). In contrast, no correlation between the expression of *Maf* and expression of the hallmark cytokine-encoding genes *Ifng* or *Il4* was observed, but, as expected, expression of these effector cytokine–encoding genes showed tight correlation with expression of *Tbx21* and *Gata3*, which encode the T_H1 cell hallmark TF T-bet and T_H2 cell hallmark TF GATA-3, respectively (Fig. 1f). Thus, c-Maf might function as a common regulator of IL-10 in CD4$^+$ T cells regardless of the T cell subset.

c-Maf deficiency in CD4$^+$ T cells affects susceptibility to disease in a context-specific manner. Having identified c-Maf as the strongest candidate as a TF regulator of IL-10, we next sought to determine whether c-Maf is a common regulator of IL-10 in vivo and to what extent c-Maf affects the immune response and associated pathologies. To this end, we investigated the effect of deletion of *Maf* targeted to CD4$^+$ T cells (*Maf*$^{fl/fl}$*Cd4*-cre) in mouse models of malaria[26] (T_H1 cells), house dust mite (HDM) allergy[27] (T_H2 cells) and experimental autoimmune encephalitis (EAE)[28] (T_H17 cells), which encapsulate a spectrum of immune responses (Fig. 2a–c). In the malaria model, *Maf*$^{fl/fl}$*Cd4*-cre mice showed greater acute-phase pathology than that of *Maf*$^{fl/fl}$ (control) mice, with significant weight loss and decrease in temperature, but c-Maf deficiency in CD4$^+$ T cells had little to no effect on parasite load (Fig. 2d). Similarly, in the HDM allergy model, *Maf*$^{fl/fl}$*Cd4*-cre mice had more total cells (mostly eosinophils) in bronchoalveolar lavage fluid and greater lung pathology (characterized by higher mucus and inflammation scores) than that of *Maf*$^{fl/fl}$ (control) mice (Fig. 2e). *Maf*$^{fl/fl}$*Cd4*-cre mice showed less pathology in the T_H17 EAE model, as demonstrated by less weight loss and lower clinical scores, with overall less-advanced disease than that of *Maf*$^{fl/fl}$ (control) mice (Fig. 2f). Our findings thus demonstrated that the disease-associated pathology that resulted from *Maf* deletion targeted to CD4$^+$ T cells was a phenocopy of that of IL-10 deficiency in the malaria model[26] and was in keeping with IL-10's regulatory role in allergy[29]. In contrast, such deletion of *Maf* in the EAE setting showed an effect opposite to that reported for IL-10[30], indicative of an additional role for c-Maf in T_H17 responses that contributed to pathology.

Deciphering c-Maf-driven transcriptional programs within dominant disease-associated immune responses. To better understand the disease-specific effects of the deletion of *Maf*, we performed RNA-seq analysis of purified CD4$^+$ T cells isolated from the spleen, lungs and the central nervous system in the three disease models noted above. Hierarchical clustering revealed that the greatest variations in gene expression were driven by each disease (Fig. 3a and Supplementary Data). However, a distinct separation of gene expression in CD4$^+$ T cells from *Maf*$^{fl/fl}$*Cd4*-cre mice from that in such cells from *Maf*$^{fl/fl}$ (control) mice was not discernible, except in the malaria model (Fig. 3a). Indeed, 78% of the variance captured by the first two singular-value-decomposition components clustered the samples according to the disease-specific immune response, as shown by biological pathway analysis (Fig. 3b–d and Supplementary Table 2). The fourth component, although it was accountable for only 3% of the variance (Fig. 3b–d and Supplementary Table 2), segregated the samples according to *Maf* deficiency, irrespective of the disease (Fig. 3b,d). This component contained both downregulated genes, including those encoding transcriptional regulators and molecules in the immune response (such as *Il10*), and upregulated genes, such as those encoding molecules with proliferative function (*E2f1, Runx3* and *Il2ra*) (Fig. 3d). Thus, although the immune response dominated over the deletion of *Maf*, c-Maf did contribute to a small but coherent change in gene expression across all three diseases in vivo that included changes in the expression of *Il10*, which confirmed the in vitro findings.

c-Maf regulates *Il10* expression in CD4$^+$ T cells in vivo with wider disease-specific effects. Subsequent comparison of genes expressed differentially in *Maf*$^{fl/fl}$*Cd4*-cre mice relative to their expression in *Maf*$^{fl/fl}$ (control) mice in all three disease models showed only 48 overlapping genes, in contrast to the overall sizable perturbation of 2,635 genes in the malaria model, 1,073 genes in the HDM allergy model and 265 genes in the EAE model, many of which were in fact disease specific and were both upregulated and downregulated in the absence of c-Maf (Fig. 4a, Supplementary Fig. 2, Supplementary Table 3 and Supplementary Data). To further characterize the context-specific effects of the deletion of *Maf*, we investigated in greater detail the differentially expressed genes encoding members of the TF, cytokine and membrane-receptor families (Fig. 4b–d and Supplementary Table 4). 12% of the genes encoding molecules involved in the immune response had known relationships with c-Maf. The majority of differences in the expression of genes encoding molecules not involved in the immune response for which c-Maf was accountable, observed predominantly in the malaria model, had not previously been recognized (Fig. 4b–d). The molecules encoded by these genes control general biological processes such as the cell cycle (*E2f1, E2f2, E2f7* and *E2f8*) or circadian rhythm (*Bhlhe40*)[31] but might nonetheless contribute to the net effect of c-Maf on the immune response.

Il10 expression was significantly lower in CD4$^+$ T cells across all three diseases in the absence of c-Maf (Fig. 4a,e–g and Supplementary Fig. 2a), as we had also demonstrated in IL-27-driven CD4$^+$ T cells and T_H17 cells in vitro (Supplementary Fig. 1a). Similarly, the production of IL-10 protein by T_H1 cells and T_H2 cells was reduced in response to deletion of *Maf* in the malaria disease model and HDM allergy disease model, respectively (Fig. 5a–d). In the EAE model, however, IL-10 protein was not detectable in CD4$^+$ T cells, in keeping with the low levels of *Il10* mRNA observed in this model (Fig. 4g). Although c-Maf had a uniform role in the induction of IL-10, it showed differing effects on hallmark TFs and cytokines[7,32,33]. In the malaria model, increased expression of *Tbx21* (Fig. 4e) and IFN-γ protein (Fig. 5,b) were observed in the absence of c-Maf, which was a phenocopy of the reported effect of the deletion of *Il10* on T_H1 responses[26]. We observed decreased expression of T_H2 cell–associated genes, including *Il4* and *Il5*, in the HDM allergy model in the absence of c-Maf (Fig. 4f). Furthermore, cells producing both IL-4 and IL-10 were 'preferentially' abolished in the HDM allergy model, as assessed by intracellular cytokine staining (Fig. 5c,d), in keeping with the increased pathology of that model (Fig. 2e). There was also decreased expression of genes associated with follicular helper T cells (T_{FH} cells), including *Bcl6* in the malaria model and *Icos* and *Il21* in both the malaria model and HDM allergy model (Fig. 4b,c), in line with published reports of the positive regulation of T_{FH} cells by c-Maf[34,35]. However, the increased pathology that we observed in the *Maf*$^{fl/fl}$*Cd4*-cre mice during the acute malaria response could not be accounted for by a decrease in T_{FH} cells, since deletion of T_{FH} cells specifically in mice with *Bcl6* deletion targeted to CD4$^+$ T cells (*Bcl6*$^{fl/fl}$*Cd4*-cre) did not affect pathology in the acute phase of malaria (Supplementary Fig. 3a) and instead affected parasitemia only in the chronic phase[36]. Moreover, we also found that IL-10 was produced mainly by non-T_{FH} cells, even as late as 15 d after infection, in the malaria model (Supplementary Fig. 3b). In the EAE model, expression of the T_H17 cell–associated genes *Rorc*, *Il17a* and *Il23r* (Fig. 4d,g) and of IL-17A protein (Fig. 5d,e) was decreased in the absence of c-Maf. We found that in the EAE model, that decrease in the T_H17 response was accompanied by increased expression of *Foxp3* mRNA (Fig. 4g) and an increased frequency of Foxp3$^+$ T_{reg} cells (Fig. 5e,f) in the

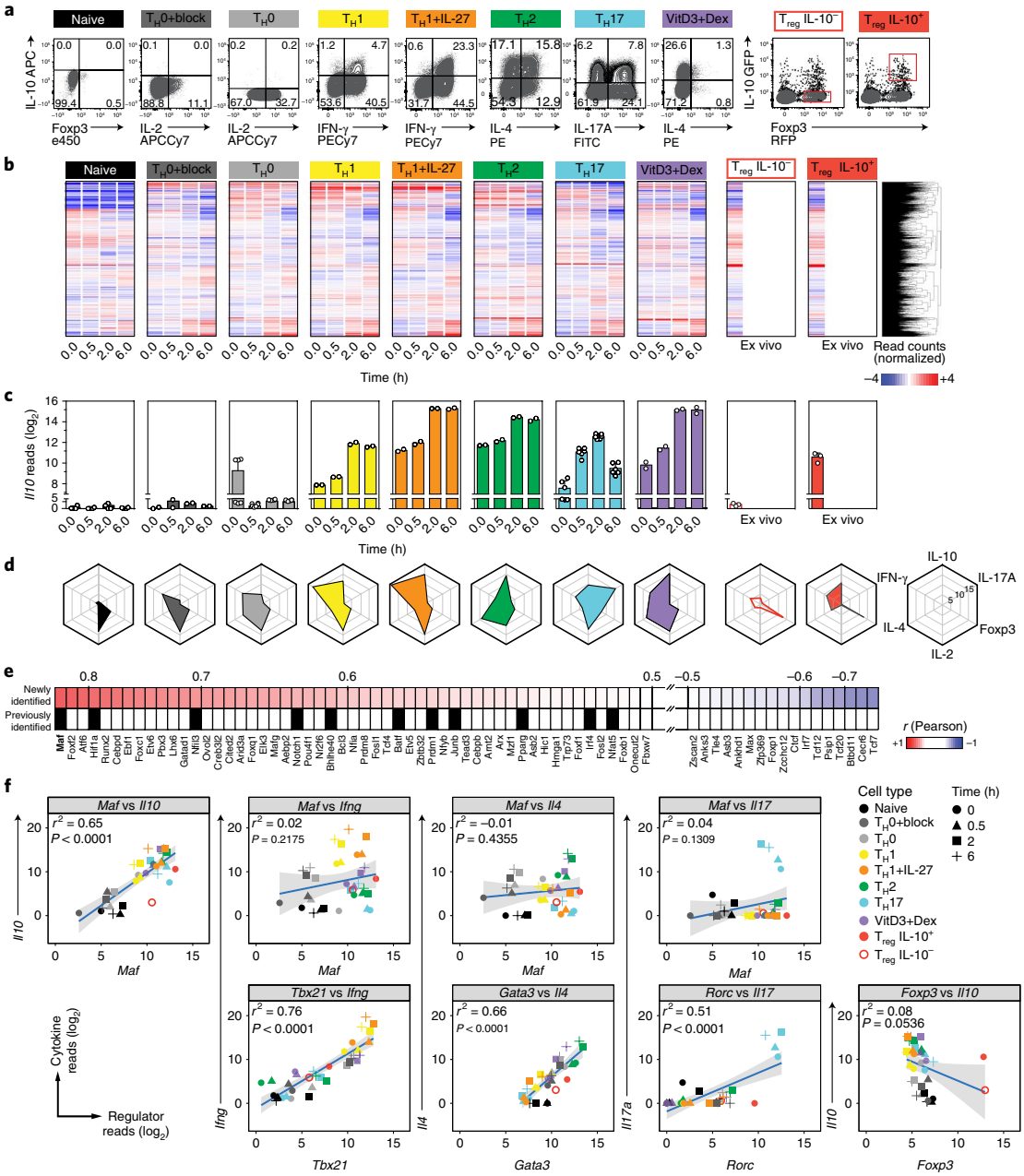

Fig. 1 | Expression of *Maf* and that of *Il10* correlate in all helper T cell and T_{reg} cell subsets. a, Flow-cytometry analysis of cytokine staining of the following cells (above plots): naive CD4$^+$ T cells (Naive); in vitro-differentiated T_H0 cells treated with antibody blockade of the cytokines IL-12p40, IFN-γ, IL-4, IL-6 and TGF-β (T_H0 + block), T_H0 cells, T_H1 cells, T_H1 cells treated with IL-27 (T_H1 + IL-27), T_H2 cells, T_H17 cells, and CD4$^+$ T cells treated with vitamin D_3 and dexamethasone (VitD3 + Dex) ($n = 2$ independent experiments per group), as well as IL-10$^-$ or IL10$^+$ T_{reg} cells ex vivo ($n = 3$ independent experiments). Numbers in quadrants indicate percent cells in each. **b**, RNA-seq analysis of CD4$^+$ T cells as in **a** (above plots), showing the mean expression (presented as read counts normalized to the median value, as baseline; key) of 12,742 genes in naive CD4$^+$ T cells ($n = 2$ independent experiments, with three culture wells in one experiment), in vitro-differentiated T_H0 cells treated with blockade as in **a** ($n = 2$ independent experiments with three culture wells in each), T_H0 cells ($n = 2$ independent experiments), T_H1 cells ($n = 2$ independent experiments), T_H1 cells treated with IL-27 ($n = 2$ independent experiments), T_H2 cells ($n = 2$ independent experiments), T_H17 cells ($n = 2$ independent experiments with three culture wells in each) and CD4$^+$ T cells treated with vitamin D_3 and dexamethasone ($n = 2$ independent experiments) after culture alone (0 h) or after 0.5, 2 or 6 h of re-stimulation in vitro (below plots), and in Foxp3$^+$ IL-10$^+$ or IL-10$^-$ T_{reg} cells ex vivo ($n = 3$ independent experiments per group). **c**,**d**, Expression of *Il10* (**c**) and of genes encoding hallmark cytokines or TFs (perimeter of key at far right) at 6 h after restimulation (**d**) in the various CD4$^+$ T cell populations in **b** (bar and shape colors in **c**,**d** match those above the plots in **b**); results in **d** are presented as the $\log_2$ value of the mean expression value per population (numbers in key at far right). Each symbol (**c**) represents an individual culture well. **e**, Positive and negative Pearson correlation (key) of the expression of genes encoding various TFs (below plot; ranked (left to right) by correlation) with the expression of *Il10* across all the CD4$^+$ T cell populations in **b** (top row); black (bottom row) indicates TFs previously associated with IL-10. **f**, Linear-regression analysis of the expression of *Maf* versus that of *Il10* or genes encoding hallmark cytokines (top row) or of the expression of genes encoding master regulators of helper T cell subsets and genes encoding hallmark cytokines (bottom row) in cells as in **b** (left key) at various times as in **b** (right key); each symbol represents the mean read counts per CD4$^+$ T cell subset per time point in **b**; shaded areas indicate the 95% confidence interval. Data are from $n = 2$ independent experiments per group (Naive, T_H0+ block, T_H0, T_H1, T_H1+IL-27, T_H2, T_H17 and VitD3+Dex) or $n = 3$ independent experiments per group (T_{reg} IL-10$^-$ and T_{reg} IL-10$^+$) (**c**–**f**; mean + s.d. in **c**).

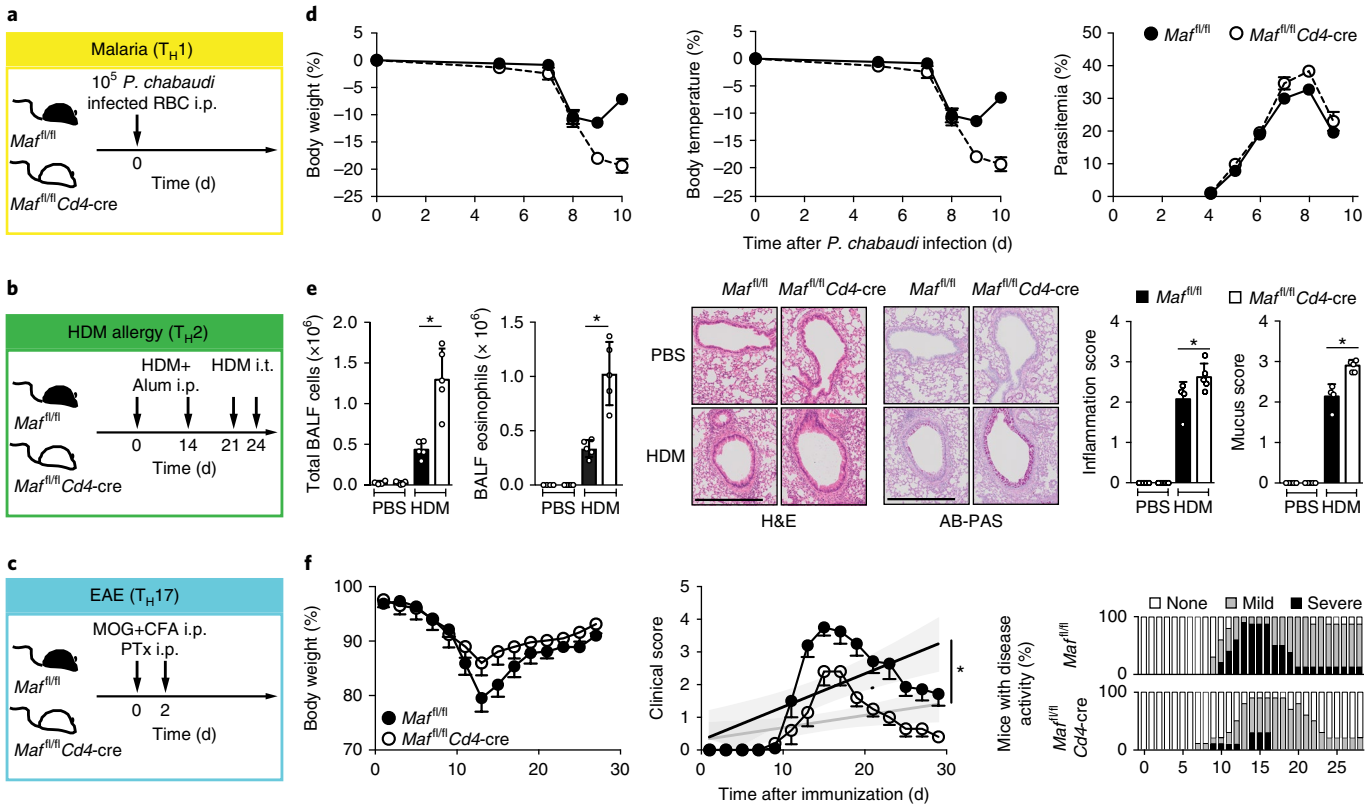

Fig. 2 | c-Maf deficiency in CD4$^+$ T cells affects susceptibility to disease in a context-specific manner. a–c, Protocol for the models with *Maf*$^{fl/fl}$ and *Maf*$^{fl/fl}$*Cd4*-cre mice: intraperitoneal (i.p.) injection of *Plasmodium chabaudi*–infected red blood cells (RBC) into mice to induce malaria (**a**); treatment of mice intraperitoneally (i.p.) with HDM in alum and intratracheally (i.t.) with HDM to induce allergy (**b**); and treatment of mice intraperitoneally (i.p.) with myelin oligodendrocyte glycoprotein (MOG) in complete Freund's adjuvant (CFA) plus pertussis toxin (PTx) to induce EAE disease (**c**). **d**, Change in body weight (left), body temperature (middle) and parasitemia (right) at various times (horizontal axis) during infection of mice (key) with *P. chabaudi* as in **a** ($n = 14$ mice per group). **e**, Total cells and eosinophils (differential counts of Giemsa-stained cells) in the bronchoalvelolar fluid (BALF) of mice (key) after treatment with PBS or HDM challenge as in **b** (horizontal axis) (left two plots; $n = 5$ experiments); microscopy of lung sections from such mice (above images and left margin), stained with H&E or with Alcian blue plus periodic acid–Schiff (AB-PAS) (below images) (middle images); and cumulative total inflammation score (from H&E analysis) and mucous score (from AB-PAS analysis) in such mice (right two plots). Each symbol (left and right) represents an individual mouse. Scale bars (middle), 500 μm. $^*P < 0.05$ (two-tailed Mann-Whitney test). **f**, Change in body weight (left) and clinical score (middle; includes linear regression) at various times (horizontal axis) during the induction of EAE as in **c** ($n = 10$ mice per group), and distribution of disease severity in such mice (right) (key: no EAE (None), score < 2; mild EAE, score = 2–3; severe EAE, score > 4; $n = 28$ mice per group). $^*P \leq 0.035$ (F-test). Data are from (**d**, **e** (left and right), **f**) or representative of (**e** (middle)) three biological replicate experiments per disease model (mean ± s.e.m. in **d**,**f**; mean ± s.d. in **e**).

absence of c-Maf. Collectively, our findings showed that in addition to controlling T_H1 and T_H2 responses, c-Maf served a previously unknown, more dominant role in the EAE model, beyond IL-10 expression, by regulating the balance of T_H17 cell responses (*Rorc*) and Foxp3$^+$ T_{reg} cell responses, which would explain the discordant disease susceptibility between the malaria model and HDM allergy model compared with the EAE model.

The context specificity of c-Maf in the immune response is driven by direct and indirect mechanisms. To identify the molecular mechanisms whereby c-Maf affects gene regulation in CD4$^+$ T cells in vivo, we used the assay for transposase-accessible chromatin plus sequencing (ATAC-seq) to reveal functionally active genomic regions. Consistent with the RNA-seq profile (Fig. 3a), hierarchical clustering of ATAC-seq data revealed that the open-chromatin landscape was dominantly driven by each disease and that a distinct separation between *Maf*-sufficient CD4$^+$ T cells and *Maf*-deficient CD4$^+$ T cells in their chromatin accessibility was observed only in the malaria model (Fig. 6a). This might potentially be explained by the finding of increased chromatin accessibility in the *Maf*$^{fl/fl}$*Cd4*-cre condition (Fig. 6b), which would in part also explain the larger number of dysregulated genes in this model (Fig. 4a). Although c-Maf did not itself show evidence of inducing chromatin remodeling (Fig. 6b), de novo motif discovery using MEME-ChIP software[37] revealed that the remodeled loci showed enrichment for Runx motif (E value = 3.8×10^{-92}) (Fig. 6b), which suggested that Runx factors might account for increased open chromatin in the malaria model through their known interactions with epigenetic modifiers[38]. However, such changes in chromatin accessibility were not exclusively responsible for the transcriptional changes observed by RNA-seq, since only a small fraction of the differentially expressed genes were associated with altered ATAC-seq peaks in any of the models (Supplementary Fig. 4). Together these data indicated that c-Maf acted via activation and repression of gene expression and that its context-specific action was defined by the accessible chromatin landscape dictated by the type of immune response.

We further integrated our RNA-seq data and ATAC-seq data with data obtained by analysis of c-Maf with chromatin immunoprecipitation followed by deep sequencing (ChIP-seq)[7] and motif data to identify genes that were targets of c-Maf; these results were confirmed by BETA software (which integrates ChIP-seq analyses and gene-expression data to identify target genes)[39] (Supplementary Fig. 5, Supplementary Table 5 and Supplementary Data). Differentially expressed genes showed enrichment for

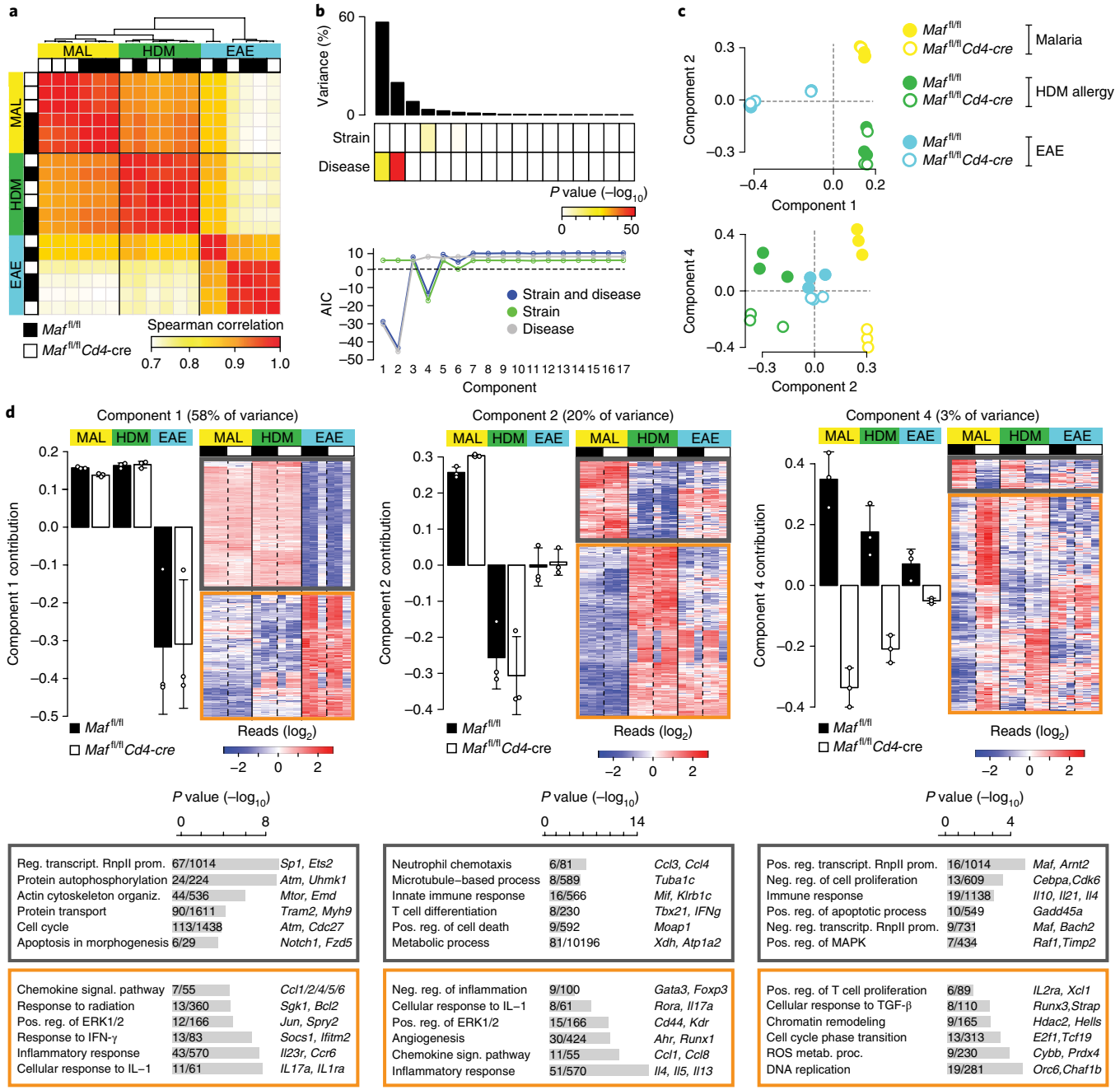

Fig. 3 | Deciphering c-Maf-driven transcriptional programs within dominant disease-associated immune responses. a, RNA-seq analysis of CD4$^+$ T cells from *Maf*$^{fl/fl}$*Cd4*-cre and *Maf*$^{fl/fl}$ mice (bottom left key) in the malaria (MAL), HDM allergy (HDM) and EAE models (left margin and above plots), presented as unsupervised hierarchical clustering showing Spearman correlation of mean gene expression (bottom right key). **b**, Singular value decomposition identifying the main sources of variation in gene expression between *Maf*$^{fl/fl}$*Cd4*-cre mice and *Maf*$^{fl/fl}$ mice in the malaria, HDM allergy and EAE models, presented as analysis of variance (ANOVA) (top plot) with the *P* value below (–$\log_{10}$ values; χ^2 test) (top half), with Akaike information criterion (AIC) then used to test the association of each component with the disease and/or strain (key) (bottom half). **c**, Separation of samples from *Maf*$^{fl/fl}$*Cd4*-cre and *Maf*$^{fl/fl}$ mice in the malaria, HDM allergy and EAE models (key) along singular-value-decomposition components 1, 2 and 4. **d**, Right-singular vectors (average values) for singular-value-decomposition component 1, 2 or 4 for each condition (top left of each group of plots); expression of the most positively (dark gray outline) and negatively (orange outline) contributing genes with the right-singular vectors of each component (top right of each group of plots); and top (most significantly over-represented) biological pathways (left margin), with the *P* value (–$\log_{10}$ values; Fisher's exact test) and number of genes within dataset/total genes annotated to a gene-ontology term (in bars), and example genes (right margin) by gene-ontology–enrichment analysis of each component (bottom). Each symbol (top left) represents an individual mouse (malaria) or a pool of up to 5 mice (HDM) or 15 mice (EAE). Data are from $n=1$ experiment (malaria) or $n=3$ experiments with $n=3$ independent mice (malaria) or $n=3$ biological replicates (HDM and EAE) per genotype (mean ± s.e.m. in **d**).

putative c-Maf-binding sites (Supplementary Table 6), which indicated that c-Maf was able to have direct effects and was responsible for the transcriptional changes seen. Specifically, the combined evidence of open chromatin coincident with binding of c-Maf to the *Il10* locus confirmed c-Maf as a direct positive regulator of *Il10* in vivo (Fig. 6c,d). However, although we found that *Il4* and *Rorc* were

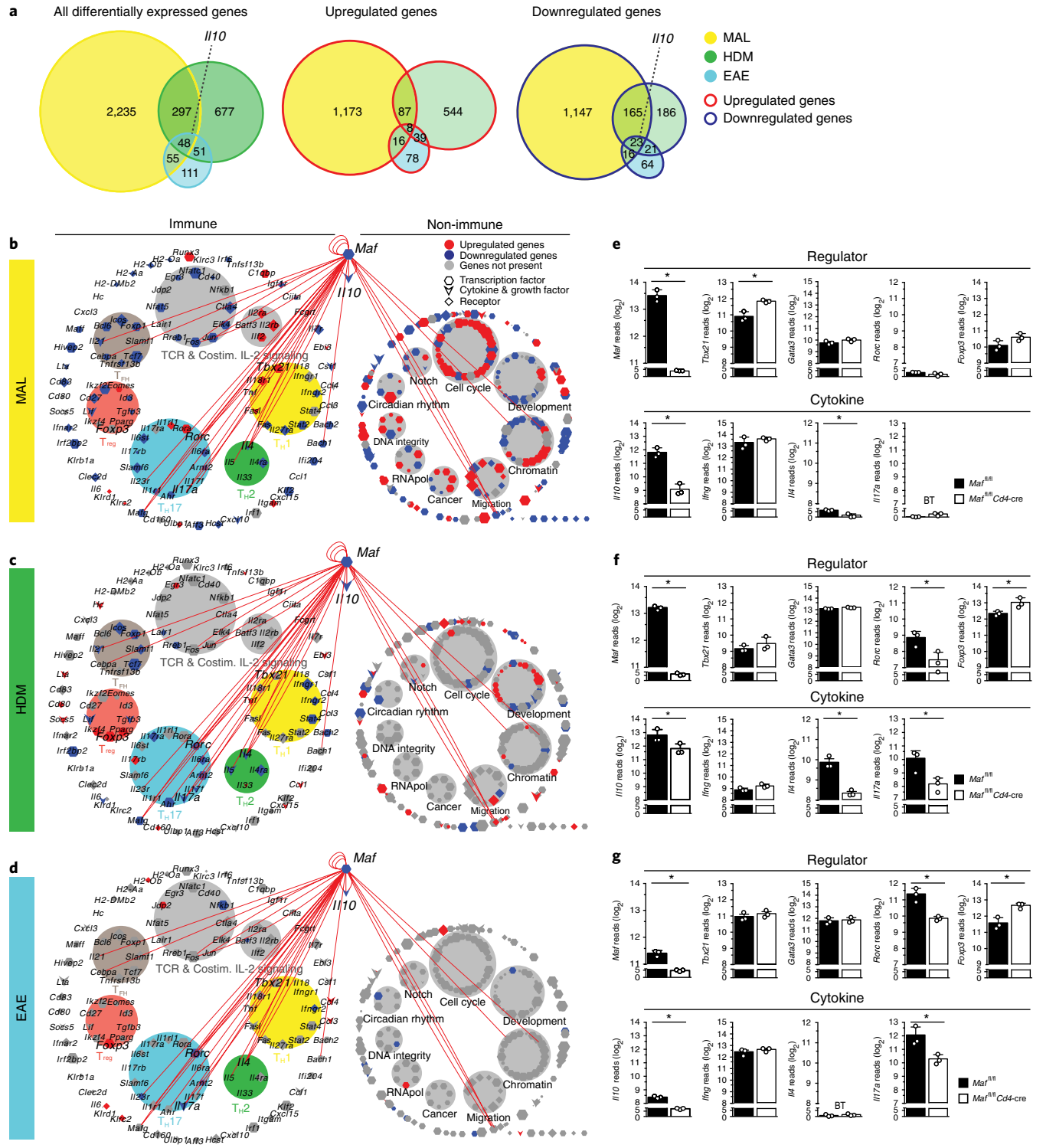

Fig. 4 | c-Maf regulates *Il10* expression in CD4$^+$ T cells in vivo with wider disease-specific effects. a, Quantification (numbers in plots) and overlap of genes differentially expressed, upregulated or downregulated (above plots) in CD4$^+$ T cells from *Maf*$^{fl/fl}$*Cd4*-cre mice relative to their expression in such cells from *Maf*$^{fl/fl}$ mice in the malaria, HDM allergy and EAE models (key), with the cutoff of an absolute change in expression of ≥1.5-fold and a *P* value of <0.05 (two-tailed moderated *t*-test). **b**–**d**, Networks of differentially expressed genes encoding TFs, cytokines and trans-membrane receptors (key), in the malaria model (**b**), HDM allergy model (**c**) and EAE model (**d**): symbol size indicates mean read number; red lines indicate known interactions with c-Maf; genes associated with T_H1 cells, T_H2 cells, T_H17 cells, T_{reg} cells and T_{FH} cells, as well as those with T cell antigen receptor (TCR) and costimulation (Costim) and IL-2 signaling, are subgrouped within the set of genes encoding molecules with immunological function. **e**–**g**, Expression of genes encoding T_H1 cell, T_H2 cell, T_H17 cell and T_{reg} cell master regulator TFs or hallmark cytokines (categories above plots) in CD4$^+$ T cells from *Maf*$^{fl/fl}$*Cd4*-cre and *Maf*$^{fl/fl}$ mice (key) in the malaria model (**e**), HDM allergy model (**f**) and EAE model (**g**), presented as normalized read counts (cutoffs as in **a**). BT, below filtering threshold. *$P < 0.05$ (two-tailed moderated *t*-test). Each symbol represents an individual mouse (malaria) or a pool of up to 5 mice (HDM) or 15 mice (EAE). Data are from $n = 1$ experiment (malaria) or $n = 3$ experiments with $n = 3$ independent mice (malaria) or $n = 3$ biological replicates (HDM and EAE) per genotype (mean ± s.d. in **e**–**g**).

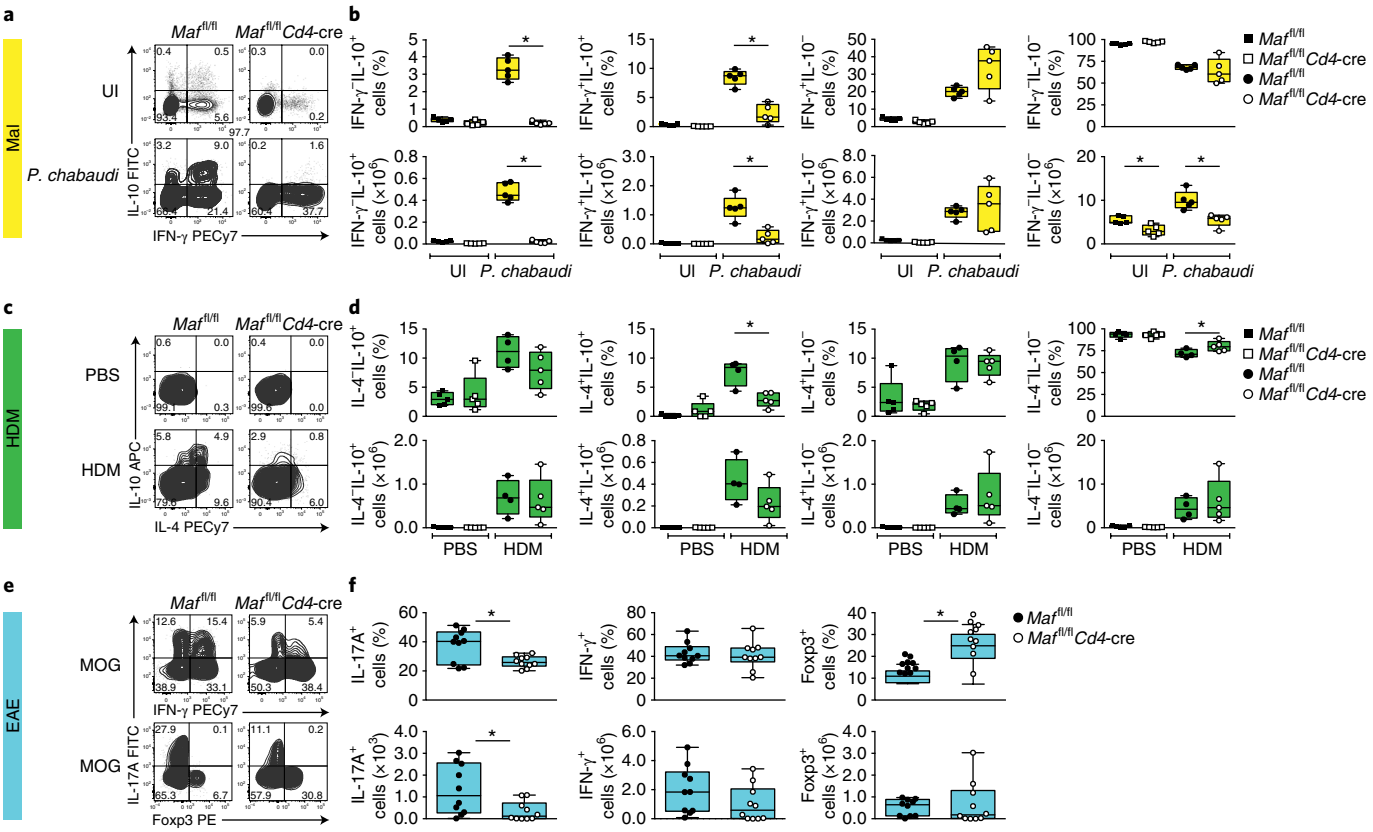

Fig. 5 | c-Maf deficiency results in the loss of IL-10-secreting effector T_H1 and T_H2 cells in the malaria and HDM allergy models, while in the EAE model, c-Maf has a dominant role in controlling the balance of T_H17 cells and T_{reg} cells. a,**c**,**e**, Flow-cytometry analysis of the cytokine staining of CD4$^+$ T cells from the spleen (**a**), lungs (**c**) or spinal cord (**e**) of *Maf*$^{fl/fl}$*Cd4*-cre and *Maf*$^{fl/fl}$ mice (above plots) left uninfected (UI) or infected with *P. Chabaudi* (left margin) in the malaria model (**a**), treated with PBS or HDM in the HDM allergy model (**c**) or treated with MOG in the EAE model (**e**), with cells gated on live CD4$^+$ T cells (**a**,**e**) or CD4$^+$CD44$^+$ T cells (**c**). **b**,**d**,**f**, Frequency (top row) and number (bottom row) of cytokine-secreting CD4$^+$ T cells in *Maf*$^{fl/fl}$*Cd4*-cre and *Maf*$^{fl/fl}$ mice (key) in the malaria model (**b**; $n = 5$ mice per group), HDM allergy model (**d**; $n = 5$ mice per group) or EAE model (**f**; $n = 10$ mice per group) treated as in **a**–**c** (below plots); box limits indicate the 25th and 75th percentiles, center line represents the median, and whiskers represent the minimum and maximum. *$P < 0.05$ (two-tailed unpaired *t*-test). Data are representative of (**a**,**c**,**e**) or from (**b**,**d**,**f**) three biological replicate experiments.

also direct targets of c-Maf, the effect of c-Maf on the expression of *Tbx21* and *Foxp3* was indirect, with no evidence of direct binding to these loci (Fig. 6c,d and Supplementary Fig. 6). Thus, the observed changes in *Rorc* expression relative to *Foxp3* expression that resulted from c-Maf deficiency were probably due to indirect mechanisms.

IL-2 is a c-Maf target. To identify candidate TFs responsible for the indirect effects of c-Maf, we applied 'bivariate genomic footprinting' (BaGFoot) software[40] to the ATAC-seq data to assess changes in global TF activity, as measured by changes in TF 'footprint depth' and accessibility of flanking motifs (Fig. 7a and Supplementary Table 7). TF-binding site motifs that were significant outliers from the multivariate distribution that showed TF binding in the absence of c-Maf different from that in its presence (the control condition) were predominantly context-specific and were more abundant in the malaria model than in the HDM allergy model or EAE model (Fig. 7a), in line with the expression data (Fig. 4a). Moreover, the accessible genomic neighborhood of differentially expressed genes showed significant enrichment for most of these TF motifs, compared with the non-differentially expressed genes (Supplementary Table 8), in the three model diseases after deletion of c-Maf. De novo motif discovery (by MEME-ChIP) identified the motif for the Runx family of TFs as the top match in differentially accessible ATAC-seq peaks in the malaria model (E value $= 3.8 \times 10^{-92}$) (Fig. 6b). The remodeled loci showed enrichment for the Runx motif (Fig. 6b), and Runx showed enhanced binding (Fig. 7a) and increased expression (Figs. 3a and 4b–d and Supplementary Table 3) in *Maf*$^{fl/fl}$*Cd4*-cre mice exclusively in the malaria model. Furthermore, Runx showed a more significant effect on differentially expressed genes than did c-Maf itself (Supplementary Table 8). Thus, Runx might have contributed to the increased pathology in the malaria model by its reported effects on IFN-γ production[41]. The AP-1 family members BATF, Jund, Jun and Junb (Fig. 7a and Supplementary Table 8), which are known to directly interact with c-Maf[42], might further contribute to changes in gene expression, including regulation of *Il10*[9]. Bhlhe40, a known negative regulator of IL-10[43] that we found was upregulated in *Maf*-deficient CD4$^+$ T cells (Supplementary Table 3), also seemed to additionally contribute to the indirect effects of c-Maf in the malaria model and HDM allergy model, as shown by the analysis with BaGFoot software (Fig. 7a and Supplementary Table 8).

In contrast to the context-specific effects on TFs, the NFAT2 motif showed significant differences in the genome-wide footprints (Fig. 7b) and contributed to changes in gene expression in all three disease models (Fig. 7a and Supplementary Table 8). On the basis of the well-known role of NFAT in the regulation of *Il2* expression[44], we concluded that both *Il2* and *Il2ra* were potential direct targets of c-Maf (Fig. 7c). Since IL-2 is known to regulate Foxp3$^+$ T_{reg} cells[5,45] and T_H17 cells[46], we postulated that the observed increase in Foxp3$^+$ T_{reg} cells and decrease in T_H17 cells in the EAE model (Figs. 4g and 5d,e) could have resulted from indirect effects of c-Maf on IL-2. To test that hypothesis and confirm the results of

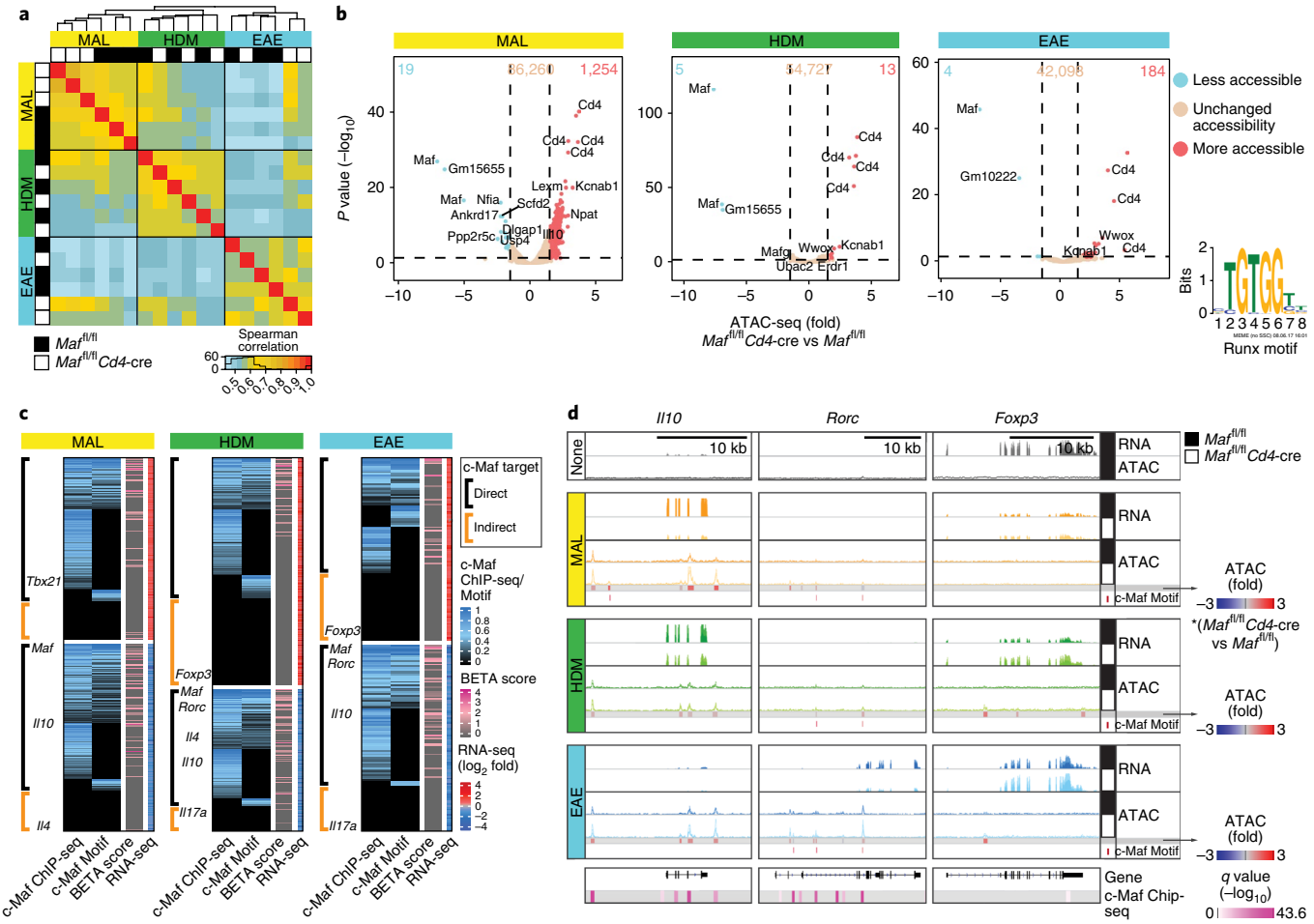

Fig. 6 | The context specificity of c-Maf in the immune response is driven by both direct mechanisms and indirect mechanisms. a, Spearman correlation (right bottom key) between read coverages underlying ATAC-seq peaks called in CD4$^+$ T cells from *Maf*$^{fl/fl}$*Cd4*-cre and *Maf*$^{fl/fl}$ mice (left bottom key) in the malaria, HDM allergy and EAE models (left margin and above plots), profiled by ATAC-seq. **b**, Change in ATAC-seq consensus peak sets in *Maf*$^{fl/fl}$*Cd4*-cre mice versus *Maf*$^{fl/fl}$ mice in the three models (above plots), presented as volcano plots (with statistical significance called (by the R Bioconductor package DiffBind 2.02) with a false-discovery rate of <0.05 and an absolute change of ≥1.5-fold); top ten peaks (with the greatest significance) ranked by false-discovery rate and change (fold values) are labeled with the assigned target gene, as well as those peaks assigned to *Il10*. **c**, ChIP-seq analysis of c-Maf, c-Maf motif analysis, BETA analysis and RNA-seq analysis (below plots; keys) of genes significantly differentially expressed in *Maf*$^{fl/fl}$*Cd4*-cre mice relative to their expression in *Maf*$^{fl/fl}$ mice, with the cutoff of an absolute change in expression of ≥1.5-fold and a *P* value of <0.05 (two-tailed moderated *t*-test) (left margin) in the malaria, HDM allergy and EAE models (above plots), showing the presence of ATAC-seq peaks with overlapping c-Maf ChIP-seq occupancy and/or c-Maf motif matches (direct target) or neither (indirect target) (bracket colors; top key), with further confirmation of putative direct and indirect targets by BETA software (lower middle key; high score represents a greater likelihood of direct regulation). **d**, Genome-browser tracks of RNA-seq and ATAC-seq read coverage (right margin) in CD4$^+$ T cells from *Maf*$^{fl/fl}$*Cd4*-cre and *Maf*$^{fl/fl}$ mice (key) left untreated (None) or in the malaria, HDM and EAE models (left margin), presented as an overlay, matched to c-Maf ChIP-seq (bottom) and c-Maf motif sites (right margin). Data are from $n=1$ experiment (malaria) or $n=3$ experiments with $n=3$ independent mice (malaria) or $n=3$ biological replicates (HDM and EAE) per genotype.

our genome-network analysis, we investigated the effect of deletion of c-Maf on *Il2* expression. *Maf*-deficient CD4$^+$ T cells had higher expression of *Il2* mRNA than that of their *Maf*-sufficient (control) counterparts under all differentiation conditions, accompanied by a reciprocal decrease in *Rorc* expression and an increase in *Foxp3* expression under T_H17 conditions and induced T_{reg} cell conditions, respectively, in vitro (Fig. 7d). The decreased expression of *Rorc* observed in *Maf*-deficient T_H17 cells was caused indirectly via the action of IL-2, since this effect was abolished by neutralization of IL-2 (Fig. 7d); this resolves published findings suggesting that c-Maf negatively regulates gene expression during T_H17 differentiation[7].

Discussion

Here we combined comprehensive transcriptional, epigenomic and TF-binding analyses of CD4$^+$ T cells from mice with *Maf*-deficiency targeted to such cells to show that c-Maf provides a common mechanism for direct transcriptional regulation of *Il10* expression in CD4$^+$ T cells in vivo in models of T_H1, T_H2 and T_H17 responses. Furthermore, we identified a broad context-specific gene-expression program regulated by c-Maf beyond its effects on IL-10, which explained the unexpected diverse effects on each disease phenotype. We demonstrated that c-Maf in fact functioned by both direct mechanisms and indirect mechanisms to regulate gene expression and to control the effector phenotype in T_H1 and T_H2 responses, which, in conjunction with IL-10, might reinforce the distinct disease outcomes observed.

In the malaria model, T_H1 cell–associated genes were regulated indirectly by a c-Maf-driven gene network that reinforces T_H1 cell activity to combat pathology. For example, *Bhlhe40*, which encodes a molecule associated with circadian rhythm[31] as well as negative

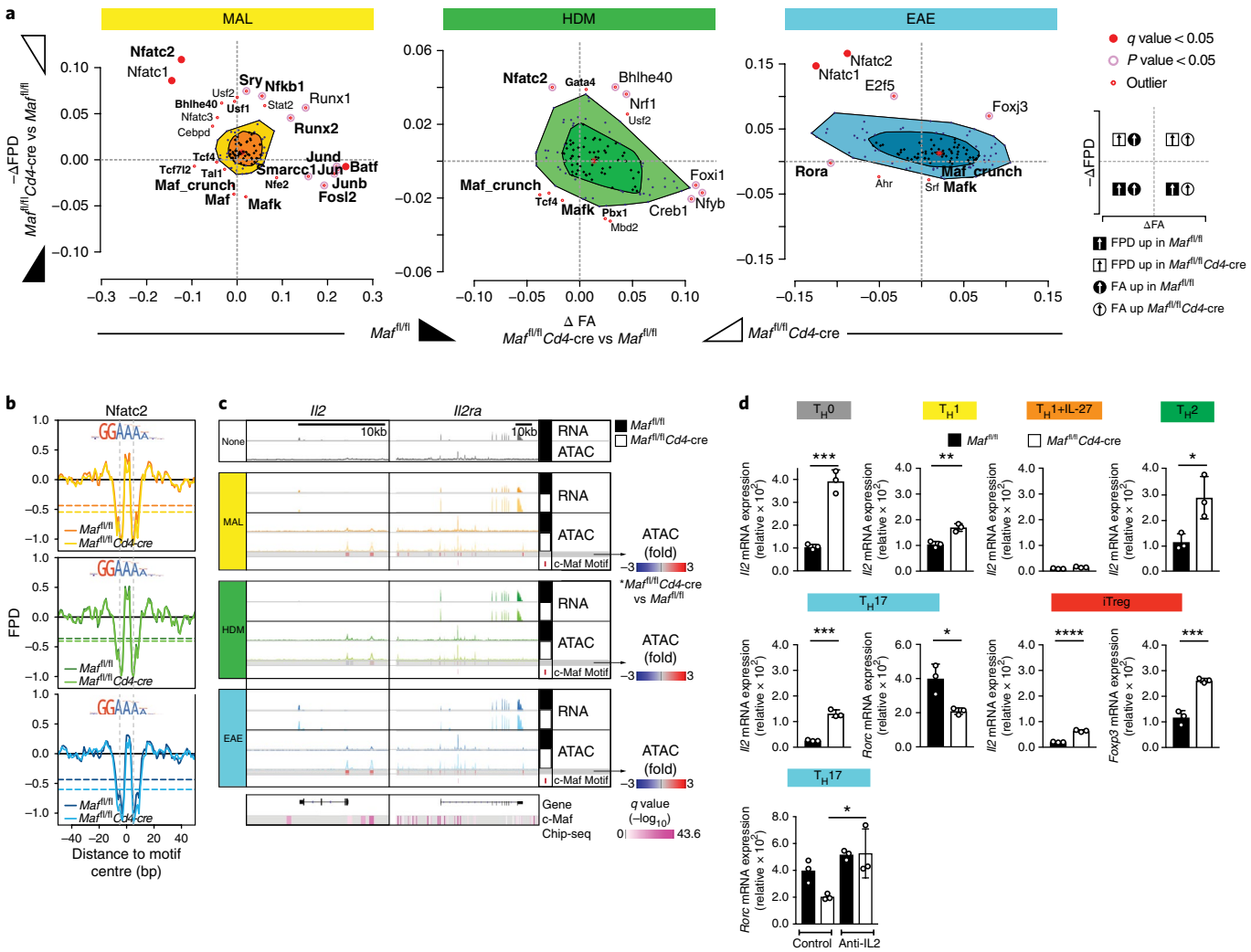

Fig. 7 | Identification and validation of IL-2 as a c-Maf target from inferred c-Maf regulated TF networks. a, BaGFoot analysis of TFs with potential genome-wide changes in binding within ATAC-seq peaks in CD4$^+$ T cells from *Maf*$^{fl/fl}$ mice relative to that in such cells from *Maf*$^{fl/fl}$*Cd4*-cre mice in the malaria, HDM allergy and EAE models (above plots), presented as the change in 'footprint depth' (−ΔFPD) plotted against the change in the accessibility of flanking motifs (change in 'flanking accessibility' (ΔFA)); wedges along axes indicate direction and degree of change in TF binding in *Maf*$^{fl/fl}$ mice (filled) and *Maf*$^{fl/fl}$*Cd4*-cre mice (open); dark shading in plot indicates a region with no change in TF motif parameters, and light shading indicates a region in which most TF motifs were located. *P* values (top key) indicate statistical confidence assigned to the differential binding of a TF in each disease model (Supplementary Data). Bold font in plot indicates TFs for which in the accessible genomic neighborhood of differentially expressed genes showed enrichment for that TF motif ($q < 0.05$ (one-tailed Fisher's exact test)). **b**, Metaprofiles of ATAC-seq footprints containing an NFATc2 motif match in CD4$^+$ T cells from *Maf*$^{fl/fl}$ and *Maf*$^{fl/fl}$*Cd4*-cre mice (key) in the malaria model (top; yellow and orange), the HDM allergy model (middle; light and dark green) and EAE model (bottom; light and dark blue): horizontal dashed lines represent the sum of transposase insertions across the footprint region in each condition; vertical dashed lines represent the motif boundaries. **c**, Genome-browser tracks of read coverage of RNA-seq and ATAC-seq in CD4$^+$ T cells from *Maf*$^{fl/fl}$*Cd4*-cre and *Maf*$^{fl/fl}$ mice (key) left untreated (None) or in the malaria, HDM allergy and EAE models (left margin), presented as an overlay, and matched to c-Maf ChIP-seq analysis (bottom) and motif sites (right margin). **d**, Expression of Il2 (all cells), *Rorc* (T_H17 cells) and *Foxp3* (induced T_{reg} cells) in naive CD4$^+$ T cells obtained from *Maf*$^{fl/fl}$ and *Maf*$^{fl/fl}$*Cd4*-cre mice and differentiated in vitro under T_H0 cell, T_H1 cell, T_H1 cell plus IL-27, T_H2 cell, T_H17 cell and induced T_{reg} cell (iT_{reg}) conditions (above plots; top eight plots) and of *Rorc* in T_H17 cells differentiated in vitro in the presence (Anti-IL-2) or absence (Control) of anti-IL-2 (bottom left); results are presented relative to those of the control gene *Hprt*. Each symbol represents an individual culture well. $^*P < 0.05$, $^{**}P < 0.01$, $^{***}P < 0.001$ and $^{****}P < 0.0001$ (two-tailed unpaired *t*-test (top eight plots) or one-way ANOVA (bottom left)). Data are from $n = 1$ experiment (malaria) or $n = 3$ experiments with $n = 3$ independent mice (malaria) or $n = 3$ biological replicates (HDM and EAE) per genotype (**a**–**c**) or are from two (T_H2) or three (all others) independent experiments with $n = 3$ culture wells per condition (**d**; mean ± s.d.).

regulation of IL-10[43], and *Runx3*, which encodes a TF key to the maximal production of IFN-γ[41] in T_H1 cells, were found to be upregulated and have increased activity in the absence of c-Maf. In contrast, we found that T_H2 cell–associated genes were direct targets of c-Maf, in keeping with its earlier definition as a positive regulator of expression of genes encoding T_H2 cell–associated cytokines[32]. However, c-Maf co-regulated IL-10 and T_H2 cell-associated genes; thus, the decrease in T_H2 cells producing both IL-4 and IL-10 observed in the absence of c-Maf might account for the overall detrimental effect on the disease pathology in the HDM allergy model.

While deletion of c-Maf resulted in increased susceptibility to disease in both the malaria model and HDM allergy model, the severity of disease was decreased in the EAE model despite reduced expression of *Il10*, indicative of additional c-Maf-regulated effects.

Further inference of c-Maf regulatory networks showed that a proportion of the transcriptional changes seen could have been a result of the increased NFAT activity observed in *Maf*-deficient CD4$^+$ T cells across all disease models. Given the well-known role of NFAT in the regulation of *Il2* expression[44] and our finding that both *Il2* and *Il2ra* were direct targets of c-Maf, we confirmed the predictions of the regulatory networks to demonstrate a role for c-Maf as a negative regulator of IL-2. Collectively our findings suggest that by negatively regulating *Il2* expression, c-Maf has overarching context-specific effects on immune responses, on the one hand limiting T_H1 and T_H2 responses that depend strongly on IL-2 and on the other hand allowing the development of a T_H17 response by regulating *Rorc* expression and Foxp3$^+$ T_{reg} cells. These findings are in apparent contrast to published studies showing that deletion of c-Maf targeted to Foxp3$^+$ cells results in fewer Rorc$^+$Foxp3$^+$ T_{reg} cells[19,20], which, given the nature of their systems, could not reveal the more global effects of c-Maf on gene expression in CD4$^+$ T cells during distinct immune responses that we have reported here. Despite that, these findings reinforce our concept that c-Maf has context-specific effects on the immune response.

Together our findings have demonstrated a broad yet context-specific role for c-Maf in regulating gene expression that allows each type of T cell effector immune response to occur in a controlled yet effective manner. Our study has also highlighted the utility of genome-wide analyses that span multiple layers of transcriptional regulation to reveal and validate gene networks.

Methods

Methods, including statements of data availability and any associated accession codes and references, are available at https://doi.org/10.1038/s41590-018-0083-5.

Received: 29 January 2018; Accepted: 8 March 2018;
Published online: 16 April 2018

References

1. Sher, A. & Coffman, R. L. Regulation of immunity to parasites by T cells and T cell-derived cytokines. *Annu. Rev. Immunol.* **10**, 385–409 (1992).
2. Littman, D. R. & Rudensky, A. Y. Th17 and regulatory T cells in mediating and restraining inflammation. *Cell* **140**, 845–858 (2010).
3. Zhu, J., Yamane, H. & Paul, W. E. Differentiation of effector CD4 T cell populations. *Annu. Rev. Immunol.* **28**, 445–489 (2010).
4. Gabrysova, L., Howes, A., Saraiva, M. & O'Garra, A. The regulation of IL-10 expression. *Curr. Top. Microbiol. Immunol.* **380**, 157–190 (2014).
5. Josefowicz, S. Z., Lu, L. F. & Rudensky, A. Y. Regulatory T cells: mechanisms of differentiation and function. *Annu. Rev. Immunol.* **30**, 531–564 (2012).
6. Apetoh, L. et al. The aryl hydrocarbon receptor interacts with c-Maf to promote the differentiation of type 1 regulatory T cells induced by IL-27. *Nat. Immunol.* **11**, 854–861 (2010).
7. Ciofani, M. et al. A validated regulatory network for Th17 cell specification. *Cell* **151**, 289–303 (2012).
8. Cipolletta, D. et al. PPAR-gamma is a major driver of the accumulation and phenotype of adipose tissue T_{reg} cells. *Nature* **486**, 549–553 (2012).
9. Jones, E. A. & Flavell, R. A. Distal enhancer elements transcribe intergenic RNA in the IL-10 family gene cluster. *J. Immunol.* **175**, 7437–7446 (2005).
10. Li, P. et al. BATF-JUN is critical for IRF4-mediated transcription in T cells. *Nature* **490**, 543–546 (2012).
11. Li, W. et al. MiR-568 inhibits the activation and function of CD4$^+$ T cells and Treg cells by targeting NFAT5. *Int. Immunol.* **26**, 269–281 (2014).
12. Mascanfroni, I. D. et al. Metabolic control of type 1 regulatory T cell differentiation by AHR and HIF1-α. *Nat. Med* **21**, 638–646 (2015).
13. Motomura, Y. et al. The transcription factor E4BP4 regulates the production of IL-10 and IL-13 in CD4$^+$ T cells. *Nat. Immunol.* **12**, 450–459 (2011).
14. Neumann, C. et al. Role of Blimp-1 in programing Th effector cells into IL-10 producers. *J. Exp. Med.* **211**, 1807–1819 (2014).
15. Rutz, S. et al. Notch regulates IL-10 production by T helper 1 cells. *Proc. Natl Acad. Sci. USA* **105**, 3497–3502 (2008).
16. Rutz, S. et al. Transcription factor c-Maf mediates the TGF-β-dependent suppression of IL-22 production in T_H17 cells. *Nat. Immunol.* 1238–1245 (2011)..
17. Tussiwand, R. et al. Compensatory dendritic cell development mediated by BATF-IRF interactions. *Nature* **490**, 502–507 (2012).
18. Wan, Y. Y. & Flavell, R. A. Identifying Foxp3-expressing suppressor T cells with a bicistronic reporter. *Proc. Natl Acad. Sci. USA* **102**, 5126–5131 (2005).
19. Wheaton, J. D., Yeh, C. H. & Ciofani, M. Cutting edge: c-Maf is required for regulatory t cells to adopt RORγt$^+$ and follicular phenotypes. *J. Immunol.* **199**, 3931–3936 (2017).
20. Xu, M. et al. c-MAF-dependent regulatory T cells mediate immunological tolerance to a gut pathobiont. *Nature* **554**, 373–377 (2018).
21. Xu, J. et al. c-Maf regulates IL-10 expression during Th17 polarization. *J. Immunol.* **182**, 6226–6236 (2009).
22. Eychene, A., Rocques, N. & Pouponnot, C. A new MAFia in cancer. *Nat. Rev. Cancer* **8**, 683–693 (2008).
23. Yoshida, H. & Hunter, C. A. The immunobiology of interleukin-27. *Annu. Rev. Immunol.* **33**, 417–443 (2015).
24. Barrat, F. J. et al. In vitro generation of interleukin 10-producing regulatory CD4$^+$ T cells is induced by immunosuppressive drugs and inhibited by T helper type 1 (Th1)- and Th2-inducing cytokines. *J. Exp. Med.* **195**, 603–616 (2002).
25. Wang, Z. Y. et al. Regulation of IL-10 gene expression in Th2 cells by Jun proteins. *J. Immunol.* **174**, 2098–2105 (2005).
26. Freitas do Rosario, A. P. et al. IL-27 promotes IL-10 production by effector Th1 CD4$^+$ T cells: a critical mechanism for protection from severe immunopathology during malaria infection. *J. Immunol.* **188**, 1178–1190 (2012).
27. Wilson, M. S. et al. Suppression of allergic airway inflammation by helminth-induced regulatory T cells. *J. Exp. Med.* **202**, 1199–1212 (2005).
28. Korn, T. et al. IL-6 controls Th17 immunity in vivo by inhibiting the conversion of conventional T cells into Foxp3+ regulatory T cells. *Proc. Natl Acad. Sci. USA* **105**, 18460–18465 (2008).
29. Coomes, S.M. et al. CD4 Th2 cells are directly regulated by IL-10 during allergic airway inflammation. *Mucosal Immunol.* **10**, 150–161 (2016).
30. Bettelli, E. et al. IL-10 is critical in the regulation of autoimmune encephalomyelitis as demonstrated by studies of IL-10- and IL-4-deficient and transgenic mice. *J. Immunol.* **161**, 3299–3306 (1998).
31. Honma, S. et al. Dec1 and Dec2 are regulators of the mammalian molecular clock. *Nature* **419**, 841–844 (2002).
32. Ho, I. C., Hodge, M. R., Rooney, J. W. & Glimcher, L. H. The proto-oncogene c-maf is responsible for tissue-specific expression of interleukin-4. *Cell* **85**, 973–983 (1996).
33. Ho, I. C., Lo, D. & Glimcher, L. H. c-maf promotes T helper cell type 2 (Th2) and attenuates Th1 differentiation by both interleukin 4-dependent and -independent mechanisms. *J. Exp. Med.* **188**, 1859–1866 (1998).
34. Andris, F. et al. The transcription factor c-Maf promotes the differentiation of follicular helper T cells. *Front. Immunol.* **8**, 480 (2017).
35. Bauquet, A. T. et al. The costimulatory molecule ICOS regulates the expression of c-Maf and IL-21 in the development of follicular T helper cells and TH-17 cells. *Nat. Immunol.* **10**, 167–175 (2009).
36. Perez-Mazliah, D. et al. Follicular helper T cells are essential for the elimination of plasmodium infection. *EBioMedicine* **24**, 216–230 (2017).
37. Ma, W., Noble, W. S. & Bailey, T. L. Motif-based analysis of large nucleotide data sets using MEME-ChIP. *Nat. Protoc.* **9**, 1428–1450 (2014).
38. Chuang, L. S., Ito, K. & Ito, Y. RUNX family: regulation and diversification of roles through interacting proteins. *Int. J. Cancer* **132**, 1260–1271 (2013).
39. Wang, S. et al. Target analysis by integration of transcriptome and ChIP-seq data with BETA. *Nat. Protoc.* **8**, 2502–2515 (2013).
40. BaekS., GoldsteinI. & HagerG. L. Bivariate genomic footprinting detects changes in transcription factor activity. *Cell Rep.* **19**, 1710–1722 (2017).
41. Djuretic, I. M. et al. Transcription factors T-bet and Runx3 cooperate to activate *Ifng* and silence *Il4* in T helper type 1 cells. *Nat. Immunol.* **8**, 145–153 (2007).
42. Kataoka, K., Noda, M. & Nishizawa, M. Maf nuclear oncoprotein recognizes sequences related to an AP-1 site and forms heterodimers with both Fos and Jun. *Mol. Cell. Biol.* **14**, 700–712 (1994).
43. Lin, C. C. et al. Bhlhe40 controls cytokine production by T cells and is essential for pathogenicity in autoimmune neuroinflammation. *Nat. Commun.* **5**, 3551 (2014).
44. Muller, M. R. & Rao, A. NFAT, immunity and cancer: a transcription factor comes of age. *Nat. Rev. Immunol.* **10**, 645–656 (2010).
45. Webster, K. E. et al. In vivo expansion of T reg cells with IL-2-mAb complexes: induction of resistance to EAE and long-term acceptance of islet allografts without immunosuppression. *J. Exp. Med.* **206**, 751–760 (2009).
46. Laurence, A. et al. Interleukin-2 signaling via STAT5 constrains T helper 17 cell generation. *Immunity* **26**, 371–381 (2007).

Acknowledgements

We thank R.A. Flavell (Yale University) for Foxp3RFP IL-10GFP mice; M. Sieweke and C. Birchmeier (Max Delbrück Centre for Molecular Medicine) for *Maf*$^{fl/fl}$ mice; G. Trinchieri (Wistar Institute) for anti-IL-12p40 (C17.8.20); The Francis Crick Institute, Biological Services for breeding and maintenance of the mice; the Advanced Sequencing

Platform and A. Sesay for help with sequence sample processing; the Flow Cytometry Platform; Bioinformatics Platform and G. Kelly for help with statistics; Photographics and M. Butt for help with figures; V. Stavropoulos for help with in vivo experiments; and A. Singhania and L. Moreira-Teixeira from the AOG laboratory for review and discussion of the manuscript. Supported by the Francis Crick Institute (Crick Core), which since 1 April 2015 has received its core funding from Cancer Research UK (FC001126 and FC010110), the UK Medical Research Council (FC001126 and FC010110) and the Wellcome Trust (FC001126 and FC010110), and before that from the UK Medical Research Council (MRC U117565642) and the European Research Council (294682-TB-PATH (Crick 10127)) (all for A.O.G., L.G., K.P., M.A.-M., L.S.C. and C.W.), the UK Medical Research Council (MRC Centenary Award for L.G.; and MRC eMedLab Medical Bioinformatics Infrastructure Award MR/L016311/1 for N.M.L.), Crick Core projects (10101 for J.L. and FC001051 for J.B. and V.M.), the Wellcome Trust (WT098326MA for J.B. and V.M.; and Joint Investigator Award 103760/Z/14/Z for N.M.L.), Inserm/CNRS and Agence Nationale de la Recherche (ANR-11-BSV3-0026), Fondation pour la Recherche Médicale (DEQ. 20110421320) and the European Research Council (695093 for M.H.S.).

Author contributions

L.G. co-designed the study with A.O.G., executed the experiments, interpreted and analyzed the data, and co-wrote the paper with A.O.G.; M.A.-M. analyzed the ATAC-seq, ChIP-seq and RNA-seq data and contributed to the writing of the paper; R.L. interpreted and analyzed the RNA-seq data and contributed to the writing of the paper; L.S.C. executed and helped design the in vitro experiments with c-Maf-deficient and control $CD4^+$ T cells and analyzed the data; J.S. and C.H. helped execute and interpret malaria experiments; D.P.-M. contributed data for Supplementary Fig. 3; C.W. helped execute EAE experiments; Y.K. and M.W. helped execute and interpret allergy experiments; K.P. performed early RNA-seq analysis; X.W. executed the genetics for obtaining *Cd4*-cre×$Maf^{fl/fl}$ mice and designed and performed all screening and quality control; L.B. performed processing and troubleshooting for RNA-seq analysis; H.W. constructed $Maf^{fl/fl}$ mice and provided feedback on the study; M.H.S. provided feedback and suggestions for the study; G.E. supervised analysis of early RNA-seq data; J.B. and V.M. provided advice and input on the ATAC-seq analysis; J.L. provided expertise for the malaria model and feedback on the study; N.M.L. provided advice and input on the RNA-seq analysis and directed the integrated analysis of ATAC-seq, ChIP-seq and RNA-seq; and A.O.G. co-designed the study with L.G., interpreted and analyzed the data, and co-wrote the paper with L.G.

Competing interests

The authors declare no competing interests.

Additional information

Supplementary information is available for this paper at https://doi.org/10.1038/s41590-018-0083-5.

Reprints and permissions information is available at www.nature.com/reprints.

Correspondence and requests for materials should be addressed to A.O.

Publisher's note: Springer Nature remains neutral with regard to jurisdictional claims in published maps and institutional affiliations.

Methods

Animals. All mice were bred and maintained under specific pathogen-free conditions at The Francis Crick Institute, Mill Hill laboratory according to the Home Office UK Animals (Scientific Procedures) Act 1986 and were used mostly at 8–12 weeks of age. C57BL/6/J wild-type mice were bred in-house. Foxp3RFP IL-10GFP mice were provided by R.A. Flavell[18,47]. *Maf*$^{fl/fl}$ mice provided by M. Sieweke and C. Birchmeier (Max Delbrück Centre for Molecular Medicine, Germany)[48], were backcrossed to C57Bl/6/J mice for ten generations and were subsequently crossed to *Cd4*-cre mice[49] to generate *Maf*$^{fl/fl}$ Cd4-cre mice, with *Maf*$^{fl/fl}$ mice used as controls. *Bcl6*$^{fl/fl}$ mice[50] were crossed to Cd4-cre mice to generate *Bcl6*$^{fl/fl}$*Cd4*-cre mice. All animal experiments were carried out in accordance with UK Home Office regulations (project licenses: malaria, 80/2358; HDM allergy, 80/2506; EAE, 70/7643) and were approved by The Francis Crick Institute Ethical Review Panel.

T cell sorting and in vitro helper T cell differentiation. Naive CD4$^+$CD62L$^+$CD44^{lo}CD25$^-$ T cells were purified from mouse spleens following negative enrichment of CD4$^+$ T cells and were sorted to over 95% purity on a MoFlo XDP cytometer (Beckman Coulter) using antibodies to the following: CD4 (RM4-5) e450, CD62L (MRL-14) PE-Cy7, CD44 (IM7) PE and CD25 (PC61.5) APC (all from eBioscience). Sorted T cells at 5×10^5 per well in flat-bottom 48-well plates were activated with plate-bound anti-CD3 (2 µg/ml, 145-2C11, Harlan) and anti-CD28 (10 µg/ml, 37.51, Harlan) and were cultured in IMDM (T_H17) or were activated with anti-CD3 (5 µg/ml) and soluble anti-CD28 (2 µg/ml) and were cultured in RPMI (other cell types) under the following conditions for 7 d unless otherwise stated: T_H0 plus blockade (T_H0 + block), anti-IL-12p40 (C17.8.20, gift from G. Trinchieri, Wistar Institute), anti-IFN-γ (XMG1.2, Harlan), anti-IL-4 (11.B.11, gift from DNAX), anti-IL-6 (MP5-20F3, gift from DNAX) and anti-TGF-β (1D11.16, gift from DNAX) at 10 µg/ml; T_H0, no cytokines or blocking antibodies added; T_H1 plus IL-27, rmIL-12p70 (5 ng/ml, BioLegend) and anti-IL-4 (identified above) with or without rmIL-27 (20 ng/ml, R&D Systems); T_H2, rmIL-4 (10 ng/ml; R&D Systems), IL-2 (5 ng/ml; Insight Biotechnology), anti-IL-12p40 (identified above) and anti-IFN-γ (identified above); T_H17, rhTGF-β1 (2 ng/ml, R&D Systems) and rhIL-6 (50 ng/ml, R&D Systems) plus anti-IFN-γ, anti-IL-4 and anti-IL-12 (all identified above) for 5 d; vitamin D_3 (40 nM, Enzo Life Sciences) and dexamethasone (10 nM, Sigma-Aldrich), plus anti-IL-4, anti-IFN-γ and anti-IL-12 (all identified above) for 21 d (VitD3 + Dex3:); and T_{reg} cells, CD4$^+$ (CD4 (RM4-5) APCe780, eBioscience) Foxp3RFP$^+$IL-10GFP$^-$ or Foxp3RFP$^+$IL-10GFP$^+$ cells were sorted directly ex vivo.

For RNA, cells were either taken at the end of the culture (0 h) or re-stimulated with anti-CD3 and anti-CD28 (both identified above) at 2 µg/ml each for 0.5, 2 and 6 h. To assess the effect of c-Maf on CD4$^+$ T cells differentiation in vitro, naive *Maf*$^{fl/fl}$*Cd4*-cre vs *Maf*$^{fl/fl}$ CD4$^+$ T cells were sorted and stimulated for up to 5 d with anti-CD3 and anti-CD28 (both identified above) at a concentration of 5 µg/ml (anti-CD3) and 2 µg/ml (anti-CD28) for culture in medium alone, with 5 ng/ml IL-12 or 25 ng/ml IL-27 or both, or with 10 ng/ml IL-4 or 50 ng/ml IL-21 or both, all in RPMI, or at a concentration of 2 µg/ml (anti-CD3) and 10 µg/ml (anti-CD28) for culture with 0.5 ng/ml TGF-β alone or with 2 ng/ml TGF-β plus 50 ng/ml IL-6 with or without 10 µg/ml anti-IL-2 (JES6-1A12, Bio X Cell), all in IMDM.

Malaria disease model. Mice (male) housed under reverse light were infected intraperitoneally with 1×10^5 *Plasmodium chabaudi chabaudi* AS infected red blood cells (RBC) obtained from donor mice with 5–10% parasitemia. Blood smears were obtained daily in the morning, when parasite sequestration is low, to best estimate the level of parasitemia; the proportion of parasitized RBCs were monitored as described previously[51]. Measurements of clinical pathology, body weight and temperature (measured using a non-invasive thermometer, Fluke), were also taken daily (PM) and results were calculated relative to the baseline at day 0. For RNA-seq and ATAC-seq, T cells were enriched by negative selection from individual spleens on day 7 after infection as described above, and Ter119$^-$CD3$^+$CD4$^+$ T cells (Ter119 (TER-119) APCCy7, BD; CD3 (145-2C11) APC, CD4 (RM4-5) e450, eBioscience) were sorted on a MoFlo XDP or BD Fusion cytometer.

House dust mite (HDM)-induced airway allergy disease model. Mice (female) were sensitized with 10 mg HDM (Greer) or PBS and 2 mg Imject Alum (Thermo Scientific) by intraperitoneal injections on days 0 and 14, and were challenged intratracheally with 10 mg HDM or PBS on days 21 and 24, as described previously[29]. On day 25, bronchoalveolar lavage was preformed, and differential cell counts were obtained following Cytospin and staining with Accustain Wright-Giemsa (Sigma-Aldrich). For histology, left lung lobes were fixed in 4% formaldehyde followed by 70% ethanol and stained with hematoxylin and eosin (inflammation) and Alcian blue plus periodic acid–Schiff (mucus). Sections were assigned scores for inflammation and mucus on a 0–4 scale as described[29], except the average score of all individual airways was calculated. For RNA-seq and ATAC-seq, CD4$^+$ T cells were enriched by positive selection (Miltenyi Biotech) from perfused lungs on day 25 following a Percoll gradient separation and CD3$^+$CD4$^+$CD44$^+$ T cells were sorted on MoFlo XDP cytometer (with antibodies to CD3 (145-2C11) APC, CD4 (RM4-5) e450 and CD44 (IM7) PE; all from eBioscience).

Experimental autoimmune encephalomyelitis (EAE) disease model. EAE was induced by immunization of mice (male or female) subcutaneously with 250 µg MOG_{35-55} peptide (Cambridge Research Biochemicals) emulsified in complete Freund's adjuvant containing 250 µg heat-killed *M. tuberculosis* H37RA (Difco Laboratories) on day 0. On days 0 and 2 after immunization, mice received 200 ng pertussis toxin (Calbiochem) intraperitoneally. Measurements of clinical pathology (body weight and clinical score) were taken daily, and results were calculated relative to the baseline at day 0. Disease severity scores were as follows: no paralysis, 0; flaccid tail, 1; impaired righting reflex and/or gait, 2; partial hindlimb paralysis, 3; complete hin limb paralysis, 4. For RNA-seq and ATAC-seq, CNS cells were enriched by Percoll gradient from perfused brains and spinal cords on days 14–16 after immunization and CD45.2$^+$CD3$^+$CD4$^+$ T cells were sorted on MoFlo^{TM} XDP cytometer (with antibodies to CD45.2 (104) APC, CD4 (RM4-5) e450 and CD4 (RM4-5) PE; all from vendor name). For RNA-seq (*Maf*$^{fl/fl}$) and ATAC-seq (C57BL/6) on untreated CD4$^+$ T cells, CD4$^+$ T cells were purified from mouse spleens following negative enrichment and CD3$^+$CD4$^+$ T cells were sorted on MoFlo XDP cytometer (with antibodies to CD3 (145-2C11) APC and CD4 (RM4-5) e450; both from eBioscience).

Flow cytometry and staining of intracellular cytokines and TFs for in vitro differentiated helper T cells. After differentiation, T cells were re-stimulated with anti-CD3 and anti-CD28 at 2 µg/ml each (both identified above) or with PDBU (Sigma-Aldrich) and ionomycin (Calbiochem) at 500 ng/ml each (T_H17) for 4 h, with brefeldin A (10 µg/ml, Sigma-Aldrich) added for the final 2 h or 4 h of culture, respectively. Surface markers were stained in PBS together with LIVE/DEAD Fixable Blue Dead Cell Stain Kit (Molecular Probes). For intracellular cytokine detection, cells were fixed with 2% formaldehyde, permeabilized with permeabilization buffer (eBioscience) and stained with the following: anti-IL-2 (JES-5H4) APC-Cy7 (BD), anti-IFN-γ (XMG1.2) PE-Cy7 (BD) and anti-IL-4 (11B11) PE, anti-IL-10 (JES5-16E3) APC and anti-IL17A (eBi17B7) FITC (all from eBioscience). For staining of Foxp3 and c-Maf, cells were fixed with Fixation/Permeabilization buffers and were stained with anti-Foxp3 (FJK-16S) PE or anti-c-Maf (symOF1) PerCP-eFluor 710 with isotype-matched control antibody IgG2bK (BMG2b) eFluor 710 (all from eBioscience).

Intracellular cytokine staining of ex vivo cells. For the malaria model, spleen cells were isolated on day 12 after infection and were restimulated with 50 ng/ml PMA and 500 ng/ml ionomycin (Sigma-Aldrich) for 4 h, with Golgi Plug (BD) added for the final 2 h of culture. Cells were then pretreated with anti-CD16/32 (2.4G2) (BD) and surface stained in PBS with anti-CD4 (RM4-5) BV605, anti-CD8 (53-6.7) BV650, anti-CD3 (145-2C11) APC-Cy7 and Zombie Aqua (all from BioLegend). After surface staining, cells were fixed with Fixation buffer followed by permeabilization in Perm Buffer (BioLegend) and were stained intracellularly with anti-IL-10 (JES5-16E3) FITC and anti-IFN-γ (XMG1.2) PE-Cy7 (both from eBioscience). T_{FH} cell staining was carried out as previously described[36].

For the HDM allergy model, lung cells were isolated from the right lower lobe on day 25 using Percoll and were restimulated with 50 ng/ml PMA and 1 mg/ml ionomycin (Sigma-Aldrich) and Golgi Stop and Plug (BD) for 6 h. Cell were then surface stained in PBS with anti-CD3 (17A2) e780, anti-CD4 (RM4-5) e450 and anti-CD44 (1M7) PerCp-Cy5.5 (all from eBioscience) in the presence of 10 µg/ml of anti-CD16/32 (2.4G2, Harlan) together with LIVE/DEAD Fixable Blue Dead Cell Stain Kit (Molecular Probes). After surface staining, cells were fixed with 2% formaldehyde, permeabilized with permeabilization buffer and stained intracellularly with IL-4 (11B11) PE-Cy7 and IL-10 (JES5-16E3) APC (both from eBioscience).

For the EAE model, cells were isolated from spinal cords and brains on day 16 after immunization using Percoll and were restimulated with 50 ng/ml PMA and 500 ng/ml ionomycin for 4 h, with brefeldin A (10 µg/ml, Sigma-Aldrich) added for the final 3 h of culture. Cells were then pretreated with 10 µg/ml of anti-CD16/32 (identified above) and surface stained in PBS with anti-CD45.2 (104) PE (eBioscience), anti-CD3 (17 A2) BV785 and anti-CD4 (RM4-5) BV605 (BioLegend), together with a LIVE/DEAD Fixable Blue Dead Cell Stain Kit (Molecular Probes). After surface staining, cells were fixed with intranuclear Fixation/Permeabilization buffers (eBioscience) and were stained with anti-IL-17A (eBi17B7) FITC, anti-Foxp3 (FJK-16S) PE (both from eBioscience) and anti-IFN-γ (XMG1.2) PE-Cy7 (BD). Samples were acquired on LSR II or Fortessa (BD) and were analyzed using FlowJo software (TreeStar).

RNA extraction and pre-processing for RNA-seq. RNA from in vitro and ex vivo CD4$^+$ T cells was extracted using an RNeasy Mini Kit according to the manufacturer's instructions (Qiagen). RNA-seq libraries were made with a TruSeq RNA Sample Preparation Kit V2 according to the manufacturer's instructions (for EAE, SMARTer Ultra^T Low Input RNA Kit v3 was used to generate cDNA that was fragmented on Covaris at 200 bp before the generation of libraries using a NuGen Ovation ultralow kit) and was sequenced using the HiSeq 2500 System with single-end read lengths of 50 bp, depth 27–65 million reads per sample (Illumina). Alignment of reads to the mouse transcriptome (mm10) and absolute quantification of the genes was performed in Strand NGS (version 2.0) with default parameters (95% identity, max 5% gaps, 1 read only if duplicated, ignoring reads

with more than five matches), guided by RefSeq annotations (2013.04.01) (in vitro helper T cells and ex vivo T_{reg} cells) or Ensembl (2014.04.01) (ex vivo $CD4^+$ T cells from the malaria, HDM allergy and EAE models). Further information on data processing is provided in the Supplementary Data.

Quantitative RT-PCR. RNA was extracted using RNAeasy microkit (Qiagen) and was reverse-transcribed into cDNA using a High Capacity Reverse Transcription kit (Applied Biosystems) according to the manufacturer's instructions, followed by RNaseH (Promega) treatment for 30 min at 37 °C. cDNA was analyzed for the expression of the following factors on a 7900HT ABI or QS3 real-time PCR system (Applied Biosystems) with the following TaqMan primer probes (all from Applied Biosystems): mouse *Maf*, Mm 02581355_s1; *Il10*, Mm00439616_m1; *Tbx21*, Mm00450960_m1; *Ifng*, Mm01168134_m1; *Gata3*, Mm00484683_m1; *Il4*, Mm00445260_m1; *Rorc*, Mm01261019_g1; *Il17a*, Mm00439619_m1; *Foxp3*, Mm 00475162_m1; *Il2*, Mm 00434256_m1; and *Il2ra*, Mm 01340213_m1. The comparative threshold cycle method with *Hrpt1*, Mm03024075_m1 as an internal control was used for the normalization of target-gene expression.

ATAC-seq. Samples were prepared as described previously[52], with the transposition reaction carried out for 1 h and 30 min at 37 °C and subsequent PCR amplification for 12 cycles. For the EAE model, 25,000 cells were used and the transposition reaction was scaled down accordingly in a reaction volume of 25 µl. Further information on data processing is provided in the Supplementary Data.

Statistical analysis. GraphPad Prism Version 6 was used to perform experimental statistical analysis. The statistical significance of differences between data groups was determined by an unpaired, two-tailed Student's *t*-test or two-tailed Mann-Whitney test where applicable at the 95% confidence level. For linear regression, correlation coefficients of determination and *P* values were calculated using the mean value of biological replicates. All sequencing data analyses were performed with the R statistical package version 3.3.1 (2016) and Bioconductor libraries version 3.3 unless otherwise stated (more information is provided in the Supplementary Data).Exact *n* values and error bars used are provided in the figure legends.

Reporting Summary. Further information on experimental design is available in the Nature Research Reporting Summary.

Data availability statement. The materials, data, code and any associated protocols that support the findings of this study are available from the corresponding author upon request. The RNA-seq and ATAC-seq datasets have been deposited in the Gene Expression Omnibus database under accession number GSE106464.

References

47. Kamanaka, M. et al. Expression of interleukin-10 in intestinal lymphocytes detected by an interleukin-10 reporter knockin tiger mouse. *Immunity* **25**, 941–952 (2006).
48. Wende, H. et al. The transcription factor c-Maf controls touch receptor development and function. *Science* **335**, 1373–1376 (2012).
49. Lee, P. P. et al. A critical role for Dnmt1 and DNA methylation in T cell development, function, and survival. *Immunity* **15**, 763–774 (2001).
50. Kaji, T. et al. Distinct cellular pathways select germline-encoded and somatically mutated antibodies into immunological memory. *J. Exp. Med.* **209**, 2079–2097 (2012).
51. Freitas do Rosario, A. P. et al. Gradual decline in malaria-specific memory T cell responses leads to failure to maintain long-term protective immunity to *Plasmodium chabaudi* AS despite persistence of B cell memory and circulating antibody. *J. Immunol.* **181**, 8344–8355 (2008).
52. Buenrostro, J. D., Giresi, P. G., Zaba, L. C., Chang, H. Y. & Greenleaf, W. J. Transposition of native chromatin for fast and sensitive epigenomic profiling of open chromatin, DNA-binding proteins and nucleosome position. *Nat. Methods* **10**, 1213–1218 (2013).

nature research

Corresponding author(s): Dr. Anne O'Garra

Life Sciences Reporting Summary

Nature Research wishes to improve the reproducibility of the work that we publish. This form is intended for publication with all accepted life science papers and provides structure for consistency and transparency in reporting. Every life science submission will use this form; some list items might not apply to an individual manuscript, but all fields must be completed for clarity.

For further information on the points included in this form, see Reporting Life Sciences Research. For further information on Nature Research policies, including our data availability policy, see Authors & Referees and the Editorial Policy Checklist.

Please do not complete any field with "not applicable" or n/a. Refer to the help text for what text to use if an item is not relevant to your study.
For final submission: please carefully check your responses for accuracy; you will not be able to make changes later.

Experimental design

1. Sample size

Describe how sample size was determined.

Animal sample size estimates were determined using previous studies and/or pilot studies using 4-5 animals per group and guided by the 3R principle.

2. Data exclusions

Describe any data exclusions.

No data exclusions were performed.

3. Replication

Describe the measures taken to verify the reproducibility of the experimental findings.

Unless otherwise stated, experimental replicates were included in analysis e.g. in RNA-Seq and ATAC-Seq analysis with appropriate statistical methods applied. Where representative data were shown, the experimental findings were reproduced with similar results.

4. Randomization

Describe how samples/organisms/participants were allocated into experimental groups.

Randomization was not carried out in this study. Animals were age and sex matched between experimental groups in order to account for covariates.

5. Blinding

Describe whether the investigators were blinded to group allocation during data collection and/or analysis.

Blinding was performed during bioinformatic data analysis, using using unsupervised methods to identify differences in transcriptomic and genomic profiles. Blinding was not performed during data collection.

Note: all in vivo studies must report how sample size was determined and whether blinding and randomization were used.

6. Statistical parameters

For all figures and tables that use statistical methods, confirm that the following items are present in relevant figure legends (or in the Methods section if additional space is needed).

n/a	Confirmed
☐	☒ The exact sample size (*n*) for each experimental group/condition, given as a discrete number and unit of measurement (animals, litters, cultures, etc.)
☐	☒ A description of how samples were collected, noting whether measurements were taken from distinct samples or whether the same sample was measured repeatedly
☐	☒ A statement indicating how many times each experiment was replicated
☐	☒ The statistical test(s) used and whether they are one- or two-sided *Only common tests should be described solely by name; describe more complex techniques in the Methods section.*
☐	☒ A description of any assumptions or corrections, such as an adjustment for multiple comparisons
☐	☒ Test values indicating whether an effect is present *Provide confidence intervals or give results of significance tests (e.g. P values) as exact values whenever appropriate and with effect sizes noted.*
☐	☒ A clear description of statistics including central tendency (e.g. median, mean) and variation (e.g. standard deviation, interquartile range)
☐	☒ Clearly defined error bars in all relevant figure captions (with explicit mention of central tendency and variation)

See the web collection on statistics for biologists for further resources and guidance.

Software

Policy information about availability of computer code

7. Software

Describe the software used to analyze the data in this study.

Flow Cytometry:
Depending on the cytometer, data was collected using either Diva or BD FACSuiteTM (BD LSR II, BD LSRFortessaTM , BD Fusion or BD FACSVerse) or Summit (MoFloTM XDP) Softwares. All data were analysed using Flow Jo software (Treestar).

Histology:
OlyVIA software was used to view and score histology slides.

RNA-Seq:
For in vitro differentiated CD4+ T cell analysis, alignment of reads to the mouse transcriptome (mm10) and absolute quantification of the genes was performed in Strand NGS (version 2.0) with default parameters (95% identity, max 5% gaps, 1 read only if duplicated, ignoring reads with more than 5 matches), guided by RefSeq annotations (2013.04.01) (in vitro TH cells) or Ensembl (2014.04.01) (ex vivo CD4+ T cells).
For ex vivo CD4+ T cell analysis, all analyses were performed with the R statistical package version 3.3.1 (2016) and Bioconductor libraries version 3.3. Proportional Venn diagrams were generated using eulerAPE webtool. Ingenuity Pathway Analysis (IPA) (QIAGEN Redwood City, www.qiagen.com/ingenuity) was used for gene family annotation and to obtain gene-gene interactions used to generate networks, which were then visualized with Cytoscape (version 3.4.0).

ATAC-Seq:
FastQC_0.11.5: for overall quality assessment
Skewer 0.2.2: sequencing quality control
IGV_2.3.97: genome browser visual inspection of ATAC-seq peaks in BED format
SAMtools 1.3.1 for alignment QC (discarded alignments with a mapQ < 30)
BWA-MEM: map pair-end reads to mm10
BEDTools 2.26.0: convert alignments from bam to bed format
Awk: command line tool. Used to remove alignments done to mitochondrial DNA, shift reads in the forward strand by + 4bp or reverse strand by -5 bp , and to remove fragments with a size >99bp.
MACS2 2.1.1: peak-calling
Diffbind 2.0.2: peak read quantification to test for differential changes in chromatin accessibility.
BaGFoot: test for differential TF activity based on changes in Tn5 insertions on motif matching sites.
DeepTools 2.4.2: bamCoverage command to retrieve RPKM normalised
IGV_2.3.97: genome browser visual inspection of ATAC-seq peaks in BED format
R statistical software for data integration and visualization.

ChIP-Seq:
Trimmomatic 0.36: sequencing quality based trimming (parameters HEADCROP:2 TRAILING:25 MINLEN:26)
Bowtie 1.1.2: map single-end reads (parameters y -m2 --best --strata -S)
BEDTools 2.26.0: convert alignments from bam to bed format
MACS2 2.1.1: peak-calling
IGV_2.3.97: genome browser visual inspection of ChIP-seq peaks in BED format
R statistical software for data integration and visualization.

Other graphs and statistics:
GraphPad Prism Version 6 was used to plot bar graphs, box and whisker graphs and line graps as well as to perform experimental statistical analysis.

For manuscripts utilizing custom algorithms or software that are central to the paper but not yet described in the published literature, software must be made available to editors and reviewers upon request. We strongly encourage code deposition in a community repository (e.g. GitHub). *Nature Methods* guidance for providing algorithms and software for publication provides further information on this topic.

Materials and reagents

Policy information about availability of materials

8. Materials availability

Indicate whether there are restrictions on availability of unique materials or if these materials are only available for distribution by a third party.

No unique materials were used in this study.

9. Antibodies

Describe the antibodies used and how they were validated for use in the system under study (i.e. assay and species).

Antibodies used in this study are as follows:

Flow cytometry:
eBioscience:
Name / Clone name/ Catalog no. / Lot no. (most recent lot no.) / dilution factor or concentration
CD4 eFluor 450 / RM4-5 / 48-0042-82 / E08484-1634 / 1:200
CD4 PE / RM4-5 / 12-0042-83 / E012640 / 1:200
CD62L PECy7 / MEL-14 / 25-0621-82 / E07577-1633 / 1:400
CD44 PE / IM7 / 12-0441-83 / E01240-1630 / 1:400
CD8 FITC / 53-6.7 / 11-0081-85 / E00116-1634 / 1:100
CD25 APC / PC61.5 / 17-0251-82 / E07106-1634 / 1:100
CD4 APC eFluor 780 / RM4-5 / 47-0042-82 / 42788618 / 1:100
Ter-119 / TER-119 / 14-5921-81 / 04582-1630 / 1:50
MHCII / M5/114.15.2 / 14-5321-85 / 4289851 / 1:50
CD11b FITC / M1/70 / 11-0112-85 / E016381 / 1:100
CD45.2 PE / 104 / 12-0454-81 / E01253-1633 / 1:200
CD3 APC / 145-2C11 / 17-0031-82 / 4283668 / 1:100
IL-17A FITC / eBi17B7 / 11-7177-81 / E00850-1632 / 1:300
Foxp3 PE / FJK-16S / 12-5773-82 / E01764-1640 / 1:200
IL-4 PE / 11B11 / 12-7041-82 / E0206-1633 / 1:100
IL-10 APC / JES5-16E3 / 17-7101-82 / E07374-1632 / 1:100
c-Maf PerCP eFluor 710 / symOF1 / 46-9855-42 / E17252-102 / 0.0075ug/test
IgG2b k isotype eFluor 710 / BMG2b / 46-4732-82 / 4291540 / 0.0075ug/test
CD3 eFluor 780 / 17A2 / 47-0032-82 / E08435-1636 / 1:200
CD44 PerCpCy5.5 / 1M7 / 45-0441-82 / E08334-1634 / 1:100
IL-4 PECy7 / 11B11 / 25-7041-82 4314701 / 1:200
IL-10 FITC / JES5-16E3 / 11-7101-82 / E033900 / 1:100
CD3 PerCpCy5.5 / 145-2C11 / 45-0031-82 / E08288-1637 / 1:200

BioLegend:
CD4 BV605 / RM4-5 / 100548 / B180158 / 1:100
CD8 BV650 / 53-6.7 / 100741 / B175409 / 1:100
CD3 BV785 / 17A2 / 100231 / B177193 / 1:400
CD3 APCCy7 / 145-2C11 / 100329 / B168040 / 1:100
CD44 FITC / IM7 / B147980 / 1:400
IL-10 FITC / JES5-16E3 / 505006 / B135115 / 1:100
CD4 APCCy7 / GK1.5 / 100414 / B159189 / 1:200
CD3 PB / 1782 / 100214 / B159411 / 1:100
PD-1 (CD279) / RMP1-30 / 109110 / B151857 / 1:200

BD:
IFNg PECy7 / XMG1.2 / 557649 / 02121 / 1:800
CD4 BD Horizon V500 / RM4-5 / 568782 / 4278618 / 1:400
Ter119 APCCy7 / TER-119 / 116223 / B191381 / 1:100
IL-2 APCCy7 / JES6-5H4 / 560547 / 7066950 / 1:500
CD16/32 purified / 2.4G2 / 553142 / 3113814 / 1:500
CXCR5 (CD185) Biotin / 2G8 / 551960 4318735 / 1:50
CCR7 e450 / 150503 / 561271 / 1 in 200
All flow cytometry antibodies were validated by the manufacturer.

Cell culture:
Harlan, custom order:
Anti-CD3 / 145-2C11 / 2 or 5 ug/ml
Anti-CD28 / 37.51 / 2 or 10 ug/ml
Anti-IFNg / XMG1.2 / 10ug/ml
Anti-CD16/32 / 24G2 / 10ug/ml

Gift antibodies from DNAX:
Anti-B220 / RA3-6A2 / 10ug/ml
Anti-CD8 / C291.2.43 / 10ug/ml
Anti-IL-4 / 11.B.11 / 10ug/ml
Anti-IL-6 / MP5-20F3 / 10ug/ml
Anti-TGFb / 1D11.16 / 10ug/ml

Gift antibody from Dr. G. Trinchieri
Anti-IL-12p40 / C17.8.20 / 10ug/ml
Cell culture antibodies were certified for cell culture by the provider.

10. Eukaryotic cell lines

a. State the source of each eukaryotic cell line used.

Cell lines were not used in this study.

b. Describe the method of cell line authentication used.

Cell lines were not used in this study.

c. Report whether the cell lines were tested for mycoplasma contamination.

Cell lines were not used in this study.

d. If any of the cell lines used are listed in the database of commonly misidentified cell lines maintained by ICLAC, provide a scientific rationale for their use.

Cell lines were not used in this study.

Animals and human research participants

Policy information about studies involving animals; when reporting animal research, follow the ARRIVE guidelines

11. Description of research animals

Provide all relevant details on animals and/or animal-derived materials used in the study.

All mice were bred and maintained under specific pathogen-free conditions at The Francis Crick Institute, Mill Hill laboratory according to the Home Office UK Animals (Scientific Procedures) Act 1986 and mostly used at 8–16 weeks of age. C57BL/6 (females) wild-type mice were bred in-house Foxp3RFP IL-10GFP (females) were provided by R.A. Flavell. C-Maffl/fl mice provided by M. Sieweke and C. Birchmeier, were backcrossed to C57Bl/6 mice for ten generations and subsequently crossed to CD4Cre mice to generate c-Maffl/flCD4Cre mice, with c-Maffl/fl mice used as controls (malaria – males, HDM allergy – females, EAE – either males or females). Bcl6fl/fl were provided by T. Takemori and crossed to CD4Cre to generate Bcl6fl/flCD4Cre mice (female). All animal experiments were carried out in accordance with UK Home Office regulations (project licenses: malaria, 80/2358; HDM allergy, 80/2506; EAE, 70/7643) and were approved by The Francis Crick Institute Ethical Review Panel.

Policy information about studies involving human research participants

12. Description of human research participants

Describe the covariate-relevant population characteristics of the human research participants.

This study does not involve human participants.

nature research

Corresponding author(s): Dr. Anne O'Garra

Flow Cytometry Reporting Summary

Form fields will expand as needed. Please do not leave fields blank.

Data presentation

For all flow cytometry data, confirm that:

☒ 1. The axis labels state the marker and fluorochrome used (e.g. CD4-FITC).

☒ 2. The axis scales are clearly visible. Include numbers along axes only for bottom left plot of group (a 'group' is an analysis of identical markers).

☒ 3. All plots are contour plots with outliers or pseudocolor plots.

☒ 4. A numerical value for number of cells or percentage (with statistics) is provided.

Methodological details

5. Describe the sample preparation.

Figure 1:
Naïve CD4+CD62L+CD44loCD25- T cells were purified from C57BL/6 mouse spleens by negative enrichment of CD4+ T cells, sorted on a MoFloTM XDP cytometer (Beckman Coulter) using CD4 e450, CD62L PECy7, CD44 PE and CD25 APC antibodies (all eBioscience) and differentiated in vitro under different TH conditions. Treg cells were sorted from IL-10GFPFoxp3RRFP dual-reporter mouse spleens directly ex vivo by negative enrichment of CD4+ T cells and sorting of CD4+ (CD4 APCe780, eBioscience) Foxp3RFP+IL-10GFP- or Foxp3RFP+IL-10GFP+ cells. After differentiation, T cells were re-stimulated with anti-CD3 and anti-CD28 at 2 ug/ml each (all TH but TH17) or PDBU (Sigma-Aldrich) and Ionomycin (Calbiochem) at 500 ng/ml each (TH17) for 4 hours, with Brefeldin A (10 ug/ml, Sigma-Aldrich) added for the last 2 or 4 hours of culture, respectively. Surface markers were stained in PBS together with LIVE/DEAD Fixable Blue Dead Cell Stain Kit (Molecular Probes). For intracellular cytokine detection, cells were fixed with 2% formaldehyde, permeabilized with permeabilization buffer (eBioscience) and stained with: anti-IL-2 APC-Cy7 (BD), anti-IFNg PECy7 (BD) and anti-IL-4 PE, anti-IL-10 APC, anti-IL17A FITC (eBioscience). For Foxp3 staining, cells were fixed with Fixation/Permeabilization buffers and stained with anti-Foxp3 PE (eBioscience).

Supplementary Figure 1:
Naïve CD4+CD62L+CD44loCD25- T cells were purified from C57BL/6 mouse spleens by negative enrichment of CD4+ T cells, sorted on a MoFloTM XDP cytometer (Beckman Coulter) using CD4 e450, CD62L PECy7, CD44 PE and CD25 APC antibodies (all eBioscience) and differentiated in vitro under different TH conditions. On day three of culture, T cells were stained in PBS with CD4 (BD Horizon V500, BD) together with LIVE/DEAD Fixable Blue Dead Cell Stain Kit (Molecular Probes). For c-Maf staining, cells were fixed with Fixation/ Permeabilization buffers and stained with c-Maf PerCP-eFluor 710 or isotype control antibodies (eBioscience).

Figures 3, 4 and 6 and accompanying Supplementary Figures:
CD4+ T cell isolation from the different disease models for subsequent RNA-Seq and ATAC-Seq analysis:
Malaria: CD4+ T cells were enriched by negative selection from individual spleens on day 7 post infection (3 individual mice c-Maffl/fl and c-Maffl/fl CD4Cre) and Ter119-CD3+CD4+ T cells (Ter119- APCCy7, CD3 APC, CD4 e450) were sorted on MoFloTM XDP MoFloTM XDP (Beckman Coulter) or BD Fusion cytometers.
HDM allergy: CD4+ T cells were enriched by positive selection (Miltenyi Biotech) from perfused lungs on day 25 (pooled from at least 5 c-Maffl/fl or c-Maffl/fl CD4Cre mice) following a Percoll gradient separation and CD3+CD4+CD44+ (CD3 APC, CD4 e450 and CD44 PE, eBioscience) T cells were sorted on MoFloTM XDP

cytometer.
EAE: CNS cells were enriched by Percoll gradient from perfused brains and spinal cords (pooled from at least 10 c-Maffl/fl or c-Maffl/fl CD4Cre mice) on day 14-16 post immunization and CD45.2+CD3+CD4+ (CD45.2 PE, CD4 e450, CD3 APC) T cells were sorted on MoFloTM XDP cytometer.

Figure 5:
CD4+ T cell intracellular cytokine staining:
Malaria; spleen cells were isolated on day 12 post infection and restimulated with 50 ng/ml PMA and 500 ng/ml Ionomycin (Sigma-Aldrich) for 4 hours, with Golgi Plug (BD) added for the last 2 hours of culture. Cells were then pretreated with anti-CD16/32 (BD) and surface stained in PBS with CD4 BV605, CD8 BV650, CD3 APCCy7 antibodies and Zombie Aqua live/dead dye (Biolegend). After surface staining, cells were fixed with Fixation buffer followed by permeabilization in Perm Buffer (Biolegend) and stained intracellularly with IL-10 FITC and IFNg PECy7 antibodies (eBioscience). For TFH cells, spleen cells were isolated on day 14 post infection and restimulated with 50 ng/ml PMA and 500 ng/ml Ionomycin (Sigma-Aldrich) for 5 hours, with with Brefeldin A (10 ug/ml, Sigma-Aldrich). Cells were then pretreated for 15 mins with anti-CD16/32 (BD) and first surface stained with anti-CXCR5-Bio (BD) in IMDM for 35 mins at 37C, washed and then stained in PBS with CD4 APCCy7, CD3 PB, CD44 PerCP-Cy5.5, PD-1 PECy7 antibodies , Streptavidin APC (Biolegend) and Zombie Aqua live/dead dye (Invitrogen) for 30 mins at 4C. After surface staining, cells were fixed with 2% paraformaldehyde for 10 mins followed by permeabilization in Perm Buffer (BD) and stained intracellularly with anti-IL-10 FITC (Biolegend).
HDM allergy; lung cells were isolated from the right lower lobe on day 25 using Percoll and restimulated with 50 ng/ml PMA and 1 mg/ml Ionomycin (Sigma-Aldrich) and Golgi Stop and Plug (BD) for 6 hours. Cell were then surface stained in PBS with CD3 APCeFluor780, CD4 eFluor450, CD44 PerCpCy5.5 antibodies (eBioscience) in the presence of anti-CD16/32 together with LIVE/DEAD Fixable Blue Dead Cell Stain Kit (Molecular Probes). After surface staining, cells were fixed with 2% formaldehyde, permeabilized with permeabilization buffer and stained intracellularly with IL-4 PECy7 and IL-10 APC antibodies (eBioscience).
EAE; cells were isolated from spinal cords and brains on day 16 post immunization using Percoll and restimulated with 50ng/ml PMA and 500 ng/ml Ionomycin for 4 hours, with Brefeldin A (10 ug/ml, Sigma-Aldrich) added for the last 3 hours of culture. Cells were then pretreated with anti-CD16/32 (10 ug/ml, Harlan) and surface stained in PBS with CD45.2 PE (eBioscience), CD3 BV785 and CD4 BV605 (Biolegend) antibodies together with LIVE/DEAD Fixable Blue Dead Cell Stain Kit (Molecular Probes). After surface staining, cells were fixed with intranuclear Fixation/Permeabilization buffers (eBioscience) and stained with IL-17A FITC, Foxp3 PE (eBioscience) and IFNg PECy7 (BD) antibodies.

6. Identify the instrument used for data collection.

Samples to be analysed were acquired on BD LSR II, BD LSRFortessaTM or BD FACSVerse (Beckton Dickinson) cytometers. Ex vivo CD4+ T cells were sorted on MoFloTM XDP (Beckman Coulter) or BD Fusion cytometers.

7. Describe the software used to collect and analyze the flow cytometry data.

Depending on the cytometer, data was collected using either Diva or BD FACSuiteTM (BD LSR II, BD LSRFortessaTM , BD Fusion or BD FACSVerse) or Summit (MoFloTM XDP) Softwares. All data were analysed using Flow Jo software (Treestar).

8. Describe the abundance of the relevant cell populations within post-sort fractions.

Naïve CD4+CD62L+CD44loCD25- were routinely sorted to over 95% purity, using a purity mode setting. Ex vivo CD4+ T cells for RNA-Seq and ATAC-Seq studies were also sorted to over 95% purity.

9. Describe the gating strategy used.

For sorting of naïve CD4+CD62L+CD44loCD25-, cells were gated on lymphocytes in FSC/SSC gate, followed by exclusion of doublets in both FSC-A/FSC-H and SSC-A/SSC-H parameters, followed by gating on live CD4+ T cells as defined by lack of PI staining in PI/CD4 eFluor 450 plot, followed by gating on CD8-CD25- cells in CD25 APC/CD8 FITC plot, followed by gating on CD62L+CD44lo cells in CD62L PECy7 / CD44 PE plot.

Ex vivo Treg cells were sorted as follows, cells were gated on lymphocytes in FSC/SSC gate, followed by exclusion of doublets in both FSC-A/FSC-H and SSC-A/SSC-H parameters, followed by gating on live CD4+ T cells as defined by lack of dead cell

dye in LIVE/DEAD Fixable Violet/CD4 APC eFluor 780 plot, followed by gating on Foxp3RFP+IL-10GFP- or Foxp3RFP+IL-10GFP+ cells.

For analysis of intracellular cytokines or proteins after in vitro differentiation, cells were gated on live CD4+ T cells as follows: lymphocytes were gated in FSC/SSC gate, followed by exclusion of doublets in both FSC-A/FSC-H and SSC-A/SSC-H parameters, followed by gating on live CD4+ T cells as defined by lack of dead cell dye in LIVE/DEAD Fixable Blue/CD4 BD Horizon V500 plot.

For sorting of CD4+ T cells from disease models ex vivo:
Malaria: Cells were gated on lymphocytes in FSC/SSC gate, followed by exclusion of doublets in FSC-A/FSC-H parameters, followed by gating on live Ter119- T cells as defined by lack of PI staining in PI/Ter119 APCCy7 plot, followed by gating on CD3 +CD4+ T cells in CD3 APC/CD4 eFluor 450 plot.
HDM: Cells were gated on lymphocytes in FSC/SSC gate, followed by exclusion of doublets in FSC-A/FSC-H parameters, followed by gating on live CD3+ T cells as defined by lack of PI staining in PI/CD3 APC plot, followed by gating on CD4+ T cells in CD4 eFluor 450/CD8 FITC plot, followed by gating on CD44+ cells in CD4 eFluor 450/CD44 PE plot.
EAE: Cells were gated on live lymphocytes in viability PI/FSC plot, followed by exclusion of doublets in both FSC-W/FSC-H and SSC-W/SSC-H parameters, followed by gating on CD45.2+ T cells in CD45.2 PE/CD11b FITC plot, followed by gating on CD3+CD4+ T cells in CD3 APC/CD4 eFluor 450 plot.

For analysis of intracellular cytokines ex vivo, cells were gated as follows:
Malaria: Lymphocytes were gated in FSC/SSC gate, followed by exclusion of doublets in both FSC-A/FSC-H and SSC-A/SSC-H parameters, followed by gating on live CD4+ T cells as defined by lack of dead cell dye in Zombie Aqua/CD3 APCCy7 plot, followed by gating on CD4+CD8- T cells in CD4 BV605/CD8 BV650 plot.
For TFH staining, Lymphocytes were gated in FSC/SSC gate, followed by exclusion of doublets in both FSC-A/FSC-H and SSC-A/SSC-H parameters, followed by gating on live CD4+CD44hi T cells as defined by lack of dead cell dye in Zombie Aqua, further gating on CD3+CD4+ T cells in CD3PB/CD4 APCCy7 plot, CD44hi PerCpCy5.5 + cells and defining the percentage of IL-10 FITC+ in CXCR5+PD-1+, CXCR5+PD-1-, CXCR5-PD-1+ and CXCR5-PD-1 populations in a CXCR5 APC/PD-1 PECy7 plot.
HDM allergy: Lymphocytes were gated in FSC/SSC gate, followed by exclusion of doublets in both FSC-A/FSC-H and SSC-A/SSC-H parameters, followed by gating on live CD4+ T cells as defined by lack of dead cell dye in LIVE/DEAD Fixable Blue /CD3 APCeFluor780 plot, followed by gating on CD4+CD44hi T cells in CD4 eFluor450/ CD44 PerCpCy5.5 plot.
EAE: Lymphocytes were gated in FSC/SSC gate, followed by exclusion of doublets in both FSC-A/FSC-H and SSC-A/SSC-H parameters, followed by gating on live CD4+ T cells as defined by lack of dead cell dye in LIVE/DEAD Fixable Blue in a histogram, followed by gating on CD3+CD4+ T cells in CD3 PerCpCy5.5/CD4 V500 plot.

Tick this box to confirm that a figure exemplifying the gating strategy is provided in the Supplementary Information. ☐

Corresponding author(s): Dr. Anne O'Garra

ChIP-seq Reporting Summary

Form fields will expand as needed. Please do not leave fields blank.

Data deposition

1. For all ChIP-seq data:

☒ a. Confirm that both raw and final processed data have been deposited in a public database such as GEO.

☒ b. Confirm that you have deposited or provided access to graph files (e.g. BED files) for the called peaks.

2. Provide all relevant data deposition access links.
The entry may remain private before publication.

* GSE106464 is the reference Series for your publication:
https://www.ncbi.nlm.nih.gov/geo/query/acc.cgi?acc=GSE106464

* This SuperSeries record provides access to all of your data and is the best accession to be quoted in any manuscript discussing the data.

* You may also cite the SubSeries that are linked to GSE106464:
(ATAC-seq) https://www.ncbi.nlm.nih.gov/geo/query/acc.cgi?acc=GSE106461
(RNA-seq in vivo) https://www.ncbi.nlm.nih.gov/geo/query/acc.cgi?acc=GSE106462
(RNA-seq in vitro) https://www.ncbi.nlm.nih.gov/geo/query/acc.cgi?acc=GSE106463

3. Provide a list of all files available in the database submission.

ATAC-Seq:
https://www.ncbi.nlm.nih.gov/geo/query/acc.cgi?acc=GSE106461

Sample name
UNT_C57BL6_1
MAL_cMaf_flfl_1
MAL_cMaf_flfl_2
MAL_cMaf_flfl_3
MAL_cMaf_flfl _CD4Cre_1
MAL_cMaf_flfl _CD4Cre_2
MAL_cMaf_flfl _CD4Cre_3
HDM_cMaf_flfl_1
HDM_cMaf_flfl_2
HDM_cMaf_flfl_3
HDM_cMaf_flfl _CD4Cre_1
HDM_cMaf_flfl _CD4Cre_2
HDM_cMaf_flfl _CD4Cre_3
EAE_cMaf_flfl _1
EAE_cMaf_flfl _2
EAE_cMaf_flfl _3
EAE_cMaf_flfl _CD4Cre_1
EAE_cMaf_flfl _CD4Cre_2
EAE_cMaf_flfl _CD4Cre_3

raw file
ATAC_UNT_C57BL6_1_GAN719A7_R1_001.fastq.gz
ATAC_MAL_cMaf_flfl_1_GAN719A3_S1_L001_R1_001.fastq.gz
ATAC_MAL_cMaf_flfl_2_GAB139A17_S6_L006_R1_001.fastq.gz
ATAC_MAL_cMaf_flfl_3_GAB139A18_S7_L007_R1_001.fastq.gz
ATAC_MAL_cMaf_flfl_CD4Cre_1_GAN719A11_S7_L007_R1_001.fastq.gz
ATAC_MAL_cMaf_flfl_CD4Cre_2_GAN719A12_S8_L008_R1_001.fastq.gz
ATAC_MAL_cMaf_flfl_CD4Cre_3_GAN719A4_S2_L002_R1_001.fastq.gz
ATAC_HDM_cMaf_flfl_1_GAN719A15_S5_L007_R1_001.fastq.gz
ATAC_HDM_cMaf_flfl_2_GAN719A17_S2_L002_R1_001.fastq.gz
ATAC_HDM_cMaf_flfl_3_GAN719A5_S3_L003_R1_001.fastq.gz

ATAC_HDM_cMaf_flfl_CD4Cre_1_GAN719A18_S3_L003_R1_001.fastq.gz
ATAC_HDM_cMaf_flfl_CD4Cre_2_GAN719A6_S4_L004_R1_001.fastq.gz
ATAC_HDM_cMaf_flfl_CD4Cre_3_GAB139A23_S37_L008_R1_001.fastq.gz
ATAC_EAE_cMaf_flfl_1_GAB139A16_S5_L005_R1_001.fastq.gz
ATAC_EAE_cMaf_flfl_2_GAB139A20_S34_L005_R1_001.fastq.gz
ATAC_EAE_cMaf_flfl_3_GAB139A22_S36_L007_R1_001.fastq.gz
ATAC_EAE_cMaf_flfl_CD4Cre_1_GAB139A15_S4_L004_R1_001.fastq.gz
ATAC_EAE_cMaf_flfl_CD4Cre_2_GAB139A19_S33_L004_R1_001.fastq.gz
ATAC_EAE_cMaf_flfl_CD4Cre_3_GAB139A21_S35_L006_R1_001.fastq.gz

raw file
ATAC_UNT_C57BL6_1_GAN719A7_R2_001.fastq.gz
ATAC_MAL_cMaf_flfl_1_GAN719A3_S1_L001_R2_001.fastq.gz
ATAC_MAL_cMaf_flfl_2_GAB139A17_S6_L006_R2_001.fastq.gz
ATAC_MAL_cMaf_flfl_3_GAB139A18_S7_L007_R2_001.fastq.gz
ATAC_MAL_cMaf_flfl_CD4Cre_1_GAN719A11_S7_L007_R2_001.fastq.gz
ATAC_MAL_cMaf_flfl_CD4Cre_2_GAN719A12_S8_L008_R2_001.fastq.gz
ATAC_MAL_cMaf_flfl_CD4Cre_3_GAN719A4_S2_L002_R2_001.fastq.gz
ATAC_HDM_cMaf_flfl_1_GAN719A15_S5_L007_R2_001.fastq.gz
ATAC_HDM_cMaf_flfl_2_GAN719A17_S2_L002_R2_001.fastq.gz
ATAC_HDM_cMaf_flfl_3_GAN719A5_S3_L003_R2_001.fastq.gz
ATAC_HDM_cMaf_flfl_CD4Cre_1_GAN719A18_S3_L003_R2_001.fastq.gz
ATAC_HDM_cMaf_flfl_CD4Cre_2_GAN719A6_S4_L004_R2_001.fastq.gz
ATAC_HDM_cMaf_flfl_CD4Cre_3_GAB139A23_S37_L008_R2_001.fastq.gz
ATAC_EAE_cMaf_flfl_1_GAB139A16_S5_L005_R2_001.fastq.gz
ATAC_EAE_cMaf_flfl_2_GAB139A20_S34_L005_R2_001.fastq.gz
ATAC_EAE_cMaf_flfl_3_GAB139A22_S36_L007_R2_001.fastq.gz
ATAC_EAE_cMaf_flfl_CD4Cre_1_GAB139A15_S4_L004_R2_001.fastq.gz
ATAC_EAE_cMaf_flfl_CD4Cre_2_GAB139A19_S33_L004_R2_001.fastq.gz
ATAC_EAE_cMaf_flfl_CD4Cre_3_GAB139A21_S35_L006_R2_001.fastq.gz

processed data file
ATAC_UNT_C57BL6_1_GAN719A7_bwa_dedup_noMt_shifted_rpkm.bw
ATAC_MAL_cMaf_flfl_1_MALARIA_GAN719A3_NoNucl_bwa_dedup_noMt_shifted_rpkm.bw
ATAC_MAL_cMaf_flfl_2_MALARIA_GAN719A21_NoNucl_bwa_dedup_noMt_shifted_rpkm.bw
ATAC_MAL_cMaf_flfl_3_MALARIA_GAN719A22_NoNucl_bwa_dedup_noMt_shifted_rpkm.bw
ATAC_MAL_cMaf_flfl_CD4Cre_1_MALARIA_GAN719A11_NoNucl_bwa_dedup_noMt_shifted_rpkm.bw
ATAC_MAL_cMaf_flfl_CD4Cre_2_MALARIA_GAN719A12_NoNucl_bwa_dedup_noMt_shifted_rpkm.bw
ATAC_MAL_cMaf_flfl_CD4Cre_3_MALARIA_GAN719A4_NoNucl_bwa_dedup_noMt_shifted_rpkm.bw
ATAC_HDM_cMaf_flfl_1_HDM_GAN719A15_NoNucl_bwa_dedup_noMt_shifted_rpkm.bw
ATAC_HDM_cMaf_flfl_2_HDM_GAN719A17_NoNucl_bwa_dedup_noMt_shifted_rpkm.bw
ATAC_HDM_cMaf_flfl_3_HDM_GAN719A5_NoNucl_bwa_dedup_noMt_shifted_rpkm.bw
ATAC_HDM_cMaf_flfl_CD4Cre_1_HDM_GAN719A18_NoNucl_bwa_dedup_noMt_shifted_rpkm.bw
ATAC_HDM_cMaf_flfl_CD4Cre_2_HDM_GAN719A6_NoNucl_bwa_dedup_noMt_shifted_rpkm.bw
ATAC_HDM_cMaf_flfl_CD4Cre_3_HDM_GAN719A27_NoNucl_bwa_dedup_noMt_shifted_rpkm.bw
ATAC_EAE_cMaf_flfl_1_EAE_GAN719A20_NoNucl_bwa_dedup_noMt_shifted_rpkm.bw
ATAC_EAE_cMaf_flfl_2_EAE_GAN719A24_NoNucl_bwa_dedup_noMt_shifted_rpkm.bw
ATAC_EAE_cMaf_flfl_3_EAE_GAN719A26_NoNucl_bwa_dedup_noMt_shifted_rpkm.bw
ATAC_EAE_cMaf_flfl_CD4Cre_1_EAE_GAN719A19_NoNucl_bwa_dedup_noMt_shifted_rpkm.bw
ATAC_EAE_cMaf_flfl_CD4Cre_2_EAE_GAN719A23_NoNucl_bwa_dedup_noMt_shi

fted_rpkm.bw
ATAC_EAE_cMaf_flfl_CD4Cre_3_EAE_GAN719A25_NoNucl_bwa_dedup_noMt_shifted_rpkm.bw

processed data file
ATAC_UNT_C57BL6_1_GAN719A7_peaks.narrowPeak
ATAC_MAL_cMaf_flfl_1_MALARIA_GAN719A3_NoNucl_peaks.narrowPeak
ATAC_MAL_cMaf_flfl_2_MALARIA_GAN719A21_NoNucl_peaks.narrowPeak
ATAC_MAL_cMaf_flfl_3_MALARIA_GAN719A22_NoNucl_peaks.narrowPeak
ATAC_MAL_cMaf_flfl_CD4Cre_1_MALARIA_GAN719A11_NoNucl_peaks.narrowPeak
ATAC_MAL_cMaf_flfl_CD4Cre_2_MALARIA_GAN719A12_NoNucl_peaks.narrowPeak
ATAC_MAL_cMaf_flfl_CD4Cre_3_MALARIA_GAN719A4_NoNucl_peaks.narrowPeak
ATAC_HDM_cMaf_flfl_1_HDM_GAN719A15_NoNucl_peaks.narrowPeak
ATAC_HDM_cMaf_flfl_2_HDM_GAN719A17_NoNucl_peaks.narrowPeak
ATAC_HDM_cMaf_flfl_3_HDM_GAN719A5_NoNucl_peaks.narrowPeak
ATAC_HDM_cMaf_flfl_CD4Cre_1_HDM_GAN719A18_NoNucl_peaks.narrowPeak
ATAC_HDM_cMaf_flfl_CD4Cre_2_HDM_GAN719A6_NoNucl_peaks.narrowPeak
ATAC_HDM_cMaf_flfl_CD4Cre_3_HDM_GAN719A27_NoNucl_peaks.narrowPeak
ATAC_EAE_cMaf_flfl_1_EAE_GAN719A20_NoNucl_peaks.narrowPeak
ATAC_EAE_cMaf_flfl_2_EAE_GAN719A24_NoNucl_peaks.narrowPeak
ATAC_EAE_cMaf_flfl_3_EAE_GAN719A26_NoNucl_peaks.narrowPeak
ATAC_EAE_cMaf_flfl_CD4Cre_1_EAE_GAN719A19_NoNucl_peaks.narrowPeak
ATAC_EAE_cMaf_flfl_CD4Cre_2_EAE_GAN719A23_NoNucl_peaks.narrowPeak
ATAC_EAE_cMaf_flfl_CD4Cre_3_EAE_GAN719A25_NoNucl_peaks.narrowPeak

RNA-seq in vivo:
https://www.ncbi.nlm.nih.gov/geo/query/acc.cgi?acc=GSE106462

Sample name
RNA_EAE_cMaf_flfl_1
RNA_EAE_cMaf_flfl_2
RNA_EAE_cMaf_flfl_3
RNA_EAE_cMaf_flfl_CD4Cre_1
RNA_EAE_cMaf_flfl_CD4Cre_2
RNA_EAE_cMaf_flfl_CD4Cre_3
RNA_HDM_cMaf_flfl_1
RNA_HDM_cMaf_flfl_2
RNA_HDM_cMaf_flfl_3
RNA_HDM_cMaf_flfl_CD4Cre_1
RNA_HDM_cMaf_flfl_CD4Cre_2
RNA_HDM_cMaf_flfl_CD4Cre_3
RNA_MAL_cMaf_flfl_1
RNA_MAL_cMaf_flfl_2
RNA_MAL_cMaf_flfl_3
RNA_MAL_cMaf_flfl_CD4Cre_1
RNA_MAL_cMaf_flfl_CD4Cre_2
RNA_MAL_cMaf_flfl_CD4Cre_3
RNA_UNT_cMaf_flfl_1
RNA_UNT_cMaf_flfl_2
RNA_UNT_cMaf_flfl_3

raw file
RNA_EAE_cMaf_flfl_1.fastq.gz
RNA_EAE_cMaf_flfl_2.fastq.gz
RNA_EAE_cMaf_flfl_3.fastq.gz
RNA_EAE_cMaf_flfl_CD4Cre_1.fastq.gz
RNA_EAE_cMaf_flfl_CD4Cre_2.fastq.gz
RNA_EAE_cMaf_flfl_CD4Cre_3.fastq.gz
RNA_HDM_cMaf_flfl_1.fastq.gz
RNA_HDM_cMaf_flfl_2.fastq.gz
RNA_HDM_cMaf_flfl_3.fastq.gz
RNA_HDM_cMaf_flfl_CD4Cre_1.fastq.gz
RNA_HDM_cMaf_flfl_CD4Cre_2.fastq.gz

RNA_HDM_cMaf_flfl_CD4Cre_3.fastq.gz
RNA_MAL_cMaf_flfl_1.fastq.gz
RNA_MAL_cMaf_flfl_2.fastq.gz
RNA_MAL_cMaf_flfl_3.fastq.gz
RNA_MAL_cMaf_flfl_CD4Cre_1.fastq.gz
RNA_MAL_cMaf_flfl_CD4Cre_2.fastq.gz
RNA_MAL_cMaf_flfl_CD4Cre_3.fastq.gz
RNA_UNT_cMaf_flfl_1.fastq.gz
RNA_UNT_cMaf_flfl_2.fastq.gz
RNA_UNT_cMaf_flfl_3.fastq.gz

processed data file
RNA_EAE_cMaf_flfl_1-All_Aligned_Reads.bw
RNA_EAE_cMaf_flfl_2-All_Aligned_Reads.bw
RNA_EAE_cMaf_flfl_3-All_Aligned_Reads.bw
RNA_EAE_cMaf_flfl_CD4Cre_1-All_Aligned_Reads.bw
RNA_EAE_cMaf_flfl_CD4Cre_2-All_Aligned_Reads.bw
RNA_EAE_cMaf_flfl_CD4Cre_3-All_Aligned_Reads.bw
RNA_HDM_cMaf_flfl_1-All_Aligned_Reads.bw
RNA_HDM_cMaf_flfl_2-All_Aligned_Reads.bw
RNA_HDM_cMaf_flfl_3-All_Aligned_Reads.bw
RNA_HDM_cMaf_flfl_CD4Cre_1-All_Aligned_Reads.bw
RNA_HDM_cMaf_flfl_CD4Cre_2-All_Aligned_Reads.bw
RNA_HDM_cMaf_flfl_CD4Cre_3-All_Aligned_Reads.bw
RNA_MAL_cMaf_flfl_1-All_Aligned_Reads.bw
RNA_MAL_cMaf_flfl_2-All_Aligned_Reads.bw
RNA_MAL_cMaf_flfl_3-All_Aligned_Reads.bw
RNA_MAL_cMaf_flfl_CD4Cre_1-All_Aligned_Reads.bw
RNA_MAL_cMaf_flfl_CD4Cre_2-All_Aligned_Reads.bw
RNA_MAL_cMaf_flfl_CD4Cre_3-All_Aligned_Reads.bw
RNA_UNT_cMaf_flfl_1-All_Aligned_Reads.bw
RNA_UNT_cMaf_flfl_2-All_Aligned_Reads.bw
RNA_UNT_cMaf_flfl_3-All_Aligned_Reads.bw

RNA-seq in vitro:
https://www.ncbi.nlm.nih.gov/geo/query/acc.cgi?acc=GSE106463

Sample name
Foxp3IL10neg_0hr_BR1_TR1_Run1
Foxp3IL10neg_0hr_BR2_TR1_Run1
Foxp3IL10neg_0hr_BR3_TR1_Run1
Foxp3IL10pos_0hr_BR1_TR1_Run1
Foxp3IL10pos_0hr_BR2_TR1_Run1
Foxp3IL10pos_0hr_BR3_TR1_Run1
Naive_0.5hr_BR1_TR1_Run1
Naive_0.5hr_BR2_TR1_Run1
Naive_0.5hr_BR2_TR2_Run1
Naive_0.5hr_BR2_TR3_Run1
Naive_0hr_BR1_TR1_Run1
Naive_0hr_BR1_TR1_Run2
Naive_0hr_BR2_TR1_Run1
Naive_0hr_BR2_TR2_Run1
Naive_0hr_BR2_TR3_Run1
Naive_2hr_BR1_TR1_Run1
Naive_2hr_BR1_TR1_Run2
Naive_2hr_BR2_TR1_Run1
Naive_2hr_BR2_TR2_Run1
Naive_2hr_BR2_TR3_Run1
Naive_6hr_BR1_TR1_Run1
Naive_6hr_BR1_TR1_Run2
Naive_6hr_BR2_TR1_Run1
Naive_6hr_BR2_TR2_Run1
Naive_6hr_BR2_TR3_Run1
TH0_0.5hr_BR1_TR1_Run1
TH0_0.5hr_BR1_TR2_Run1
TH0_0.5hr_BR1_TR3_Run1

TH0_0.5hr_BR2_TR1_Run1
TH0_0.5hr_BR2_TR2_Run1
TH0_0.5hr_BR2_TR3_Run1
TH0_0hr_BR1_TR1_Run1
TH0_0hr_BR1_TR2_Run1
TH0_0hr_BR1_TR3_Run1
TH0_0hr_BR2_TR1_Run1
TH0_0hr_BR2_TR2_Run1
TH0_0hr_BR2_TR3_Run1
TH0_2hr_BR1_TR1_Run1
TH0_2hr_BR1_TR2_Run1
TH0_2hr_BR1_TR3_Run1
TH0_2hr_BR2_TR1_Run1
TH0_2hr_BR2_TR2_Run1
TH0_2hr_BR2_TR3_Run1
TH0_6hr_BR1_TR1_Run1
TH0_6hr_BR1_TR2_Run1
TH0_6hr_BR1_TR3_Run1
TH0_6hr_BR2_TR1_Run1
TH0_6hr_BR2_TR2_Run1
TH0_6hr_BR2_TR3_Run1
TH0block_0.5hr_BR1_TR1_Run1
TH0block_0.5hr_BR1_TR1_Run2
TH0block_0.5hr_BR2_TR1_Run1
TH0block_0.5hr_BR2_TR1_Run2
TH0block_0hr_BR1_TR1_Run1
TH0block_0hr_BR1_TR1_Run2
TH0block_0hr_BR2_TR1_Run1
TH0block_0hr_BR2_TR1_Run2
TH0block_2hr_BR1_TR1_Run1
TH0block_2hr_BR1_TR1_Run2
TH0block_2hr_BR2_TR1_Run1
TH0block_2hr_BR2_TR1_Run2
TH0block_6hr_BR1_TR1_Run1
TH0block_6hr_BR1_TR1_Run2
TH0block_6hr_BR2_TR1_Run1
TH0block_6hr_BR2_TR1_Run2
TH1_0.5hr_BR1_TR1_Run1
TH1_0.5hr_BR2_TR1_Run1
TH1_0.5hr_BR2_TR1_Run2
TH1_0hr_BR1_TR1_Run1
TH1_0hr_BR2_TR1_Run1
TH1_0hr_BR2_TR1_Run2
TH1_2hr_BR1_TR1_Run1
TH1_2hr_BR2_TR1_Run1
TH1_2hr_BR2_TR1_Run2
TH1_6hr_BR1_TR1_Run1
TH1_6hr_BR2_TR1_Run1
TH1_6hr_BR2_TR1_Run2
TH17_0.5hr_BR1_TR1_Run1
TH17_0.5hr_BR1_TR2_Run1
TH17_0.5hr_BR1_TR3_Run1
TH17_0.5hr_BR2_TR1_Run1
TH17_0.5hr_BR2_TR2_Run1
TH17_0.5hr_BR2_TR3_Run1
TH17_0hr_BR1_TR1_Run1
TH17_0hr_BR1_TR2_Run1
TH17_0hr_BR1_TR3_Run1
TH17_0hr_BR2_TR1_Run1
TH17_0hr_BR2_TR2_Run1
TH17_0hr_BR2_TR3_Run1
TH17_2hr_BR1_TR1_Run1
TH17_2hr_BR1_TR2_Run1
TH17_2hr_BR1_TR3_Run1
TH17_2hr_BR2_TR1_Run1
TH17_2hr_BR2_TR2_Run1

TH17_2hr_BR2_TR3_Run1
TH17_6hr_BR1_TR1_Run1
TH17_6hr_BR1_TR2_Run1
TH17_6hr_BR1_TR3_Run1
TH17_6hr_BR2_TR1_Run1
TH17_6hr_BR2_TR2_Run1
TH17_6hr_BR2_TR3_Run1
TH1IL27_0.5hr_BR1_TR1_Run1
TH1IL27_0.5hr_BR2_TR1_Run1
TH1IL27_0hr_BR1_TR1_Run1
TH1IL27_0hr_BR2_TR1_Run1
TH1IL27_2hr_BR1_TR1_Run1
TH1IL27_2hr_BR2_TR1_Run1
TH1IL27_6hr_BR1_TR1_Run1
TH1IL27_6hr_BR2_TR1_Run1
TH2_0.5hr_BR1_TR1_Run1
TH2_0.5hr_BR1_TR1_Run2
TH2_0.5hr_BR2_TR1_Run1
TH2_0.5hr_BR2_TR1_Run2
TH2_0hr_BR1_TR1_Run1
TH2_0hr_BR1_TR1_Run2
TH2_0hr_BR2_TR1_Run1
TH2_0hr_BR2_TR1_Run2
TH2_2hr_BR1_TR1_Run1
TH2_2hr_BR1_TR1_Run2
TH2_2hr_BR2_TR1_Run1
TH2_2hr_BR2_TR1_Run2
TH2_6hr_BR1_TR1_Run1
TH2_6hr_BR2_TR1_Run1
TH2_6hr_BR2_TR1_Run2
VitDex_0.5hr_BR1_TR1_Run1
VitDex_0.5hr_BR1_TR1_Run2
VitDex_0.5hr_BR2_TR1_Run1
VitDex_0hr_BR1_TR1_Run1
VitDex_0hr_BR2_TR1_Run1
VitDex_2hr_BR1_TR1_Run1
VitDex_2hr_BR1_TR1_Run2
VitDex_2hr_BR2_TR1_Run1
VitDex_6hr_BR1_TR1_Run1
VitDex_6hr_BR2_TR1_Run1

raw file
Foxp3IL10neg_0hr_BR1_TR1_Run1.fastq.gz
Foxp3IL10neg_0hr_BR2_TR1_Run1.fastq.gz
Foxp3IL10neg_0hr_BR3_TR1_Run1.fastq.gz
Foxp3IL10pos_0hr_BR1_TR1_Run1.fastq.gz
Foxp3IL10pos_0hr_BR2_TR1_Run1.fastq.gz
Foxp3IL10pos_0hr_BR3_TR1_Run1.fastq.gz
Naive_0.5hr_BR1_TR1_Run1.fastq.gz
Naive_0.5hr_BR2_TR1_Run1.fastq.gz
Naive_0.5hr_BR2_TR2_Run1.fastq.gz
Naive_0.5hr_BR2_TR3_Run1.fastq.gz
Naive_0hr_BR1_TR1_Run1.fastq.gz
Naive_0hr_BR1_TR1_Run2.fastq.gz
Naive_0hr_BR2_TR1_Run1.fastq.gz
Naive_0hr_BR2_TR2_Run1.fastq.gz
Naive_0hr_BR2_TR3_Run1.fastq.gz
Naive_2hr_BR1_TR1_Run1.fastq.gz
Naive_2hr_BR1_TR1_Run2.fastq.gz
Naive_2hr_BR2_TR1_Run1.fastq.gz
Naive_2hr_BR2_TR2_Run1.fastq.gz
Naive_2hr_BR2_TR3_Run1.fastq.gz
Naive_6hr_BR1_TR1_Run1.fastq.gz
Naive_6hr_BR1_TR1_Run2.fastq.gz
Naive_6hr_BR2_TR1_Run1.fastq.gz
Naive_6hr_BR2_TR2_Run1.fastq.gz

Naive_6hr_BR2_TR3_Run1.fastq.gz
TH0_0.5hr_BR1_TR1_Run1.fastq.gz
TH0_0.5hr_BR1_TR2_Run1.fastq.gz
TH0_0.5hr_BR1_TR3_Run1.fastq.gz
TH0_0.5hr_BR2_TR1_Run1.fastq.gz
TH0_0.5hr_BR2_TR2_Run1.fastq.gz
TH0_0.5hr_BR2_TR3_Run1.fastq.gz
TH0_0hr_BR1_TR1_Run1.fastq.gz
TH0_0hr_BR1_TR2_Run1.fastq.gz
TH0_0hr_BR1_TR3_Run1.fastq.gz
TH0_0hr_BR2_TR1_Run1.fastq.gz
TH0_0hr_BR2_TR2_Run1.fastq.gz
TH0_0hr_BR2_TR3_Run1.fastq.gz
TH0_2hr_BR1_TR1_Run1.fastq.gz
TH0_2hr_BR1_TR2_Run1.fastq.gz
TH0_2hr_BR1_TR3_Run1.fastq.gz
TH0_2hr_BR2_TR1_Run1.fastq.gz
TH0_2hr_BR2_TR2_Run1.fastq.gz
TH0_2hr_BR2_TR3_Run1.fastq.gz
TH0_6hr_BR1_TR1_Run1.fastq.gz
TH0_6hr_BR1_TR2_Run1.fastq.gz
TH0_6hr_BR1_TR3_Run1.fastq.gz
TH0_6hr_BR2_TR1_Run1.fastq.gz
TH0_6hr_BR2_TR2_Run1.fastq.gz
TH0_6hr_BR2_TR3_Run1.fastq.gz
TH0block_0.5hr_BR1_TR1_Run1.fastq.gz
TH0block_0.5hr_BR1_TR1_Run2.fastq.gz
TH0block_0.5hr_BR2_TR1_Run1.fastq.gz
TH0block_0.5hr_BR2_TR1_Run2.fastq.gz
TH0block_0hr_BR1_TR1_Run1.fastq.gz
TH0block_0hr_BR1_TR1_Run2.fastq.gz
TH0block_0hr_BR2_TR1_Run1.fastq.gz
TH0block_0hr_BR2_TR1_Run2.fastq.gz
TH0block_2hr_BR1_TR1_Run1.fastq.gz
TH0block_2hr_BR1_TR1_Run2.fastq.gz
TH0block_2hr_BR2_TR1_Run1.fastq.gz
TH0block_2hr_BR2_TR1_Run2.fastq.gz
TH0block_6hr_BR1_TR1_Run1.fastq.gz
TH0block_6hr_BR1_TR1_Run2.fastq.gz
TH0block_6hr_BR2_TR1_Run1.fastq.gz
TH0block_6hr_BR2_TR1_Run2.fastq.gz
TH1_0.5hr_BR1_TR1_Run1.fastq.gz
TH1_0.5hr_BR2_TR1_Run1.fastq.gz
TH1_0.5hr_BR2_TR1_Run2.fastq.gz
TH1_0hr_BR1_TR1_Run1.fastq.gz
TH1_0hr_BR2_TR1_Run1.fastq.gz
TH1_0hr_BR2_TR1_Run2.fastq.gz
TH1_2hr_BR1_TR1_Run1.fastq.gz
TH1_2hr_BR2_TR1_Run1.fastq.gz
TH1_2hr_BR2_TR1_Run2.fastq.gz
TH1_6hr_BR1_TR1_Run1.fastq.gz
TH1_6hr_BR2_TR1_Run1.fastq.gz
TH1_6hr_BR2_TR1_Run2.fastq.gz
TH17_0.5hr_BR1_TR1_Run1.fastq.gz
TH17_0.5hr_BR1_TR2_Run1.fastq.gz
TH17_0.5hr_BR1_TR3_Run1.fastq.gz
TH17_0.5hr_BR2_TR1_Run1.fastq.gz
TH17_0.5hr_BR2_TR2_Run1.fastq.gz
TH17_0.5hr_BR2_TR3_Run1.fastq.gz
TH17_0hr_BR1_TR1_Run1.fastq.gz
TH17_0hr_BR1_TR2_Run1.fastq.gz
TH17_0hr_BR1_TR3_Run1.fastq.gz
TH17_0hr_BR2_TR1_Run1.fastq.gz
TH17_0hr_BR2_TR2_Run1.fastq.gz
TH17_0hr_BR2_TR3_Run1.fastq.gz
TH17_2hr_BR1_TR1_Run1.fastq.gz

TH17_2hr_BR1_TR2_Run1.fastq.gz
TH17_2hr_BR1_TR3_Run1.fastq.gz
TH17_2hr_BR2_TR1_Run1.fastq.gz
TH17_2hr_BR2_TR2_Run1.fastq.gz
TH17_2hr_BR2_TR3_Run1.fastq.gz
TH17_6hr_BR1_TR1_Run1.fastq.gz
TH17_6hr_BR1_TR2_Run1.fastq.gz
TH17_6hr_BR1_TR3_Run1.fastq.gz
TH17_6hr_BR2_TR1_Run1.fastq.gz
TH17_6hr_BR2_TR2_Run1.fastq.gz
TH17_6hr_BR2_TR3_Run1.fastq.gz
TH1IL27_0.5hr_BR1_TR1_Run1.fastq.gz
TH1IL27_0.5hr_BR2_TR1_Run1.fastq.gz
TH1IL27_0hr_BR1_TR1_Run1.fastq.gz
TH1IL27_0hr_BR2_TR1_Run1.fastq.gz
TH1IL27_2hr_BR1_TR1_Run1.fastq.gz
TH1IL27_2hr_BR2_TR1_Run1.fastq.gz
TH1IL27_6hr_BR1_TR1_Run1.fastq.gz
TH1IL27_6hr_BR2_TR1_Run1.fastq.gz
TH2_0.5hr_BR1_TR1_Run1.fastq.gz
TH2_0.5hr_BR1_TR1_Run2.fastq.gz
TH2_0.5hr_BR2_TR1_Run1.fastq.gz
TH2_0.5hr_BR2_TR1_Run2.fastq.gz
TH2_0hr_BR1_TR1_Run1.fastq.gz
TH2_0hr_BR1_TR1_Run2.fastq.gz
TH2_0hr_BR2_TR1_Run1.fastq.gz
TH2_0hr_BR2_TR1_Run2.fastq.gz
TH2_2hr_BR1_TR1_Run1.fastq.gz
TH2_2hr_BR1_TR1_Run2.fastq.gz
TH2_2hr_BR2_TR1_Run1.fastq.gz
TH2_2hr_BR2_TR1_Run2.fastq.gz
TH2_6hr_BR1_TR1_Run1.fastq.gz
TH2_6hr_BR2_TR1_Run1.fastq.gz
TH2_6hr_BR2_TR1_Run2.fastq.gz
VitDex_0.5hr_BR1_TR1_Run1.fastq.gz
VitDex_0.5hr_BR1_TR1_Run2.fastq.gz
VitDex_0.5hr_BR2_TR1_Run1.fastq.gz
VitDex_0hr_BR1_TR1_Run1.fastq.gz
VitDex_0hr_BR2_TR1_Run1.fastq.gz
VitDex_2hr_BR1_TR1_Run1.fastq.gz
VitDex_2hr_BR1_TR1_Run2.fastq.gz
VitDex_2hr_BR2_TR1_Run1.fastq.gz
VitDex_6hr_BR1_TR1_Run1.fastq.gz
VitDex_6hr_BR2_TR1_Run1.fastq.gz

processed data file
Foxp3IL10neg_0hr_BR1_TR1-All_Aligned_Reads.bw
Foxp3IL10neg_0hr_BR2_TR1-All_Aligned_Reads.bw
Foxp3IL10neg_0hr_BR3_TR1-All_Aligned_Reads.bw
Foxp3IL10pos_0hr_BR1_TR1-All_Aligned_Reads.bw
Foxp3IL10pos_0hr_BR2_TR1-All_Aligned_Reads.bw
Foxp3IL10pos_0hr_BR3_TR1-All_Aligned_Reads.bw
Naive_0.5hr_BR1_TR1-All_Aligned_Reads.bw
Naive_0.5hr_BR2_TR1-All_Aligned_Reads.bw
Naive_0.5hr_BR2_TR2-All_Aligned_Reads.bw
Naive_0.5hr_BR2_TR3-All_Aligned_Reads.bw
Naive_0hr_BR1_TR1-All_Aligned_Reads.bw
Naive_0hr_BR1_TR1-All_Aligned_Reads.bw
Naive_0hr_BR2_TR1-All_Aligned_Reads.bw
Naive_0hr_BR2_TR2-All_Aligned_Reads.bw
Naive_0hr_BR2_TR3-All_Aligned_Reads.bw
Naive_2hr_BR1_TR1-All_Aligned_Reads.bw
Naive_2hr_BR1_TR1-All_Aligned_Reads.bw
Naive_2hr_BR2_TR1-All_Aligned_Reads.bw
Naive_2hr_BR2_TR2-All_Aligned_Reads.bw
Naive_2hr_BR2_TR3-All_Aligned_Reads.bw

Naive_6hr_BR1_TR1-All_Aligned_Reads.bw
Naive_6hr_BR1_TR1-All_Aligned_Reads.bw
Naive_6hr_BR2_TR1-All_Aligned_Reads.bw
Naive_6hr_BR2_TR2-All_Aligned_Reads.bw
Naive_6hr_BR2_TR3-All_Aligned_Reads.bw
TH0_0.5hr_BR1_TR1-All_Aligned_Reads.bw
TH0_0.5hr_BR1_TR2-All_Aligned_Reads.bw
TH0_0.5hr_BR1_TR3-All_Aligned_Reads.bw
TH0_0.5hr_BR2_TR1-All_Aligned_Reads.bw
TH0_0.5hr_BR2_TR2-All_Aligned_Reads.bw
TH0_0.5hr_BR2_TR3-All_Aligned_Reads.bw
TH0_0hr_BR1_TR1-All_Aligned_Reads.bw
TH0_0hr_BR1_TR2-All_Aligned_Reads.bw
TH0_0hr_BR1_TR3-All_Aligned_Reads.bw
TH0_0hr_BR2_TR1-All_Aligned_Reads.bw
TH0_0hr_BR2_TR2-All_Aligned_Reads.bw
TH0_0hr_BR2_TR3-All_Aligned_Reads.bw
TH0_2hr_BR1_TR1-All_Aligned_Reads.bw
TH0_2hr_BR1_TR2-All_Aligned_Reads.bw
TH0_2hr_BR1_TR3-All_Aligned_Reads.bw
TH0_2hr_BR2_TR1-All_Aligned_Reads.bw
TH0_2hr_BR2_TR2-All_Aligned_Reads.bw
TH0_2hr_BR2_TR3-All_Aligned_Reads.bw
TH0_6hr_BR1_TR1-All_Aligned_Reads.bw
TH0_6hr_BR1_TR2-All_Aligned_Reads.bw
TH0_6hr_BR1_TR3-All_Aligned_Reads.bw
TH0_6hr_BR2_TR1-All_Aligned_Reads.bw
TH0_6hr_BR2_TR2-All_Aligned_Reads.bw
TH0_6hr_BR2_TR3-All_Aligned_Reads.bw
TH0block_0.5hr_BR1_TR1-All_Aligned_Reads.bw
TH0block_0.5hr_BR1_TR1-All_Aligned_Reads.bw
TH0block_0.5hr_BR2_TR1-All_Aligned_Reads.bw
TH0block_0.5hr_BR2_TR1-All_Aligned_Reads.bw
TH0block_0hr_BR1_TR1-All_Aligned_Reads.bw
TH0block_0hr_BR1_TR1-All_Aligned_Reads.bw
TH0block_0hr_BR2_TR1-All_Aligned_Reads.bw
TH0block_0hr_BR2_TR1-All_Aligned_Reads.bw
TH0block_2hr_BR1_TR1-All_Aligned_Reads.bw
TH0block_2hr_BR1_TR1-All_Aligned_Reads.bw
TH0block_2hr_BR2_TR1-All_Aligned_Reads.bw
TH0block_2hr_BR2_TR1-All_Aligned_Reads.bw
TH0block_6hr_BR1_TR1-All_Aligned_Reads.bw
TH0block_6hr_BR1_TR1-All_Aligned_Reads.bw
TH0block_6hr_BR2_TR1-All_Aligned_Reads.bw
TH0block_6hr_BR2_TR1-All_Aligned_Reads.bw
TH1_0.5hr_BR1_TR1-All_Aligned_Reads.bw
TH1_0.5hr_BR2_TR1-All_Aligned_Reads.bw
TH1_0.5hr_BR2_TR1-All_Aligned_Reads.bw
TH1_0hr_BR1_TR1-All_Aligned_Reads.bw
TH1_0hr_BR2_TR1-All_Aligned_Reads.bw
TH1_0hr_BR2_TR1-All_Aligned_Reads.bw
TH1_2hr_BR1_TR1-All_Aligned_Reads.bw
TH1_2hr_BR2_TR1-All_Aligned_Reads.bw
TH1_2hr_BR2_TR1-All_Aligned_Reads.bw
TH1_6hr_BR1_TR1-All_Aligned_Reads.bw
TH1_6hr_BR2_TR1-All_Aligned_Reads.bw
TH1_6hr_BR2_TR1-All_Aligned_Reads.bw
TH17_0.5hr_BR1_TR1-All_Aligned_Reads.bw
TH17_0.5hr_BR1_TR2-All_Aligned_Reads.bw
TH17_0.5hr_BR1_TR3-All_Aligned_Reads.bw
TH17_0.5hr_BR2_TR1-All_Aligned_Reads.bw
TH17_0.5hr_BR2_TR2-All_Aligned_Reads.bw
TH17_0.5hr_BR2_TR3-All_Aligned_Reads.bw
TH17_0hr_BR1_TR1-All_Aligned_Reads.bw
TH17_0hr_BR1_TR2-All_Aligned_Reads.bw
TH17_0hr_BR1_TR3-All_Aligned_Reads.bw

TH17_0hr_BR2_TR1-All_Aligned_Reads.bw
TH17_0hr_BR2_TR2-All_Aligned_Reads.bw
TH17_0hr_BR2_TR3-All_Aligned_Reads.bw
TH17_2hr_BR1_TR1-All_Aligned_Reads.bw
TH17_2hr_BR1_TR2-All_Aligned_Reads.bw
TH17_2hr_BR1_TR3-All_Aligned_Reads.bw
TH17_2hr_BR2_TR1-All_Aligned_Reads.bw
TH17_2hr_BR2_TR2-All_Aligned_Reads.bw
TH17_2hr_BR2_TR3-All_Aligned_Reads.bw
TH17_6hr_BR1_TR1-All_Aligned_Reads.bw
TH17_6hr_BR1_TR2-All_Aligned_Reads.bw
TH17_6hr_BR1_TR3-All_Aligned_Reads.bw
TH17_6hr_BR2_TR1-All_Aligned_Reads.bw
TH17_6hr_BR2_TR2-All_Aligned_Reads.bw
TH17_6hr_BR2_TR3-All_Aligned_Reads.bw
TH1IL27_0.5hr_BR1_TR1-All_Aligned_Reads.bw
TH1IL27_0.5hr_BR2_TR1-All_Aligned_Reads.bw
TH1IL27_0hr_BR1_TR1-All_Aligned_Reads.bw
TH1IL27_0hr_BR2_TR1-All_Aligned_Reads.bw
TH1IL27_2hr_BR1_TR1-All_Aligned_Reads.bw
TH1IL27_2hr_BR2_TR1-All_Aligned_Reads.bw
TH1IL27_6hr_BR1_TR1-All_Aligned_Reads.bw
TH1IL27_6hr_BR2_TR1-All_Aligned_Reads.bw
TH2_0.5hr_BR1_TR1-All_Aligned_Reads.bw
TH2_0.5hr_BR1_TR1-All_Aligned_Reads.bw
TH2_0.5hr_BR2_TR1-All_Aligned_Reads.bw
TH2_0.5hr_BR2_TR1-All_Aligned_Reads.bw
TH2_0hr_BR1_TR1-All_Aligned_Reads.bw
TH2_0hr_BR1_TR1-All_Aligned_Reads.bw
TH2_0hr_BR2_TR1-All_Aligned_Reads.bw
TH2_0hr_BR2_TR1-All_Aligned_Reads.bw
TH2_2hr_BR1_TR1-All_Aligned_Reads.bw
TH2_2hr_BR1_TR1-All_Aligned_Reads.bw
TH2_2hr_BR2_TR1-All_Aligned_Reads.bw
TH2_2hr_BR2_TR1-All_Aligned_Reads.bw
TH2_6hr_BR1_TR1-All_Aligned_Reads.bw
TH2_6hr_BR2_TR1-All_Aligned_Reads.bw
TH2_6hr_BR2_TR1-All_Aligned_Reads.bw
VitDex_0.5hr_BR1_TR1-All_Aligned_Reads.bw
VitDex_0.5hr_BR1_TR1-All_Aligned_Reads.bw
VitDex_0.5hr_BR2_TR1-All_Aligned_Reads.bw
VitDex_0hr_BR1_TR1-All_Aligned_Reads.bw
VitDex_0hr_BR2_TR1-All_Aligned_Reads.bw
VitDex_2hr_BR1_TR1-All_Aligned_Reads.bw
VitDex_2hr_BR1_TR1-All_Aligned_Reads.bw
VitDex_2hr_BR2_TR1-All_Aligned_Reads.bw
VitDex_6hr_BR1_TR1-All_Aligned_Reads.bw
VitDex_6hr_BR2_TR1-All_Aligned_Reads.bw

4. Provide a link to an anonymized genome browser session (e.g. UCSC), if available.

Not available.

Methodological details

5. Describe the experimental replicates.

The Assay for Transposase Accessible Chromatin with high-throughput sequencing (ATAC-seq) was carried out on CD4+ T cells from each of the three disease models (Malaria, HDM allergy, and EAE). There were three biological replicates for each of the two genotypes (c-Maffl/fl and c-Maf fl/fl CD4Cre).

6. Describe the sequencing depth for each experiment.

All ATAC-seq samples were sequenced using Illumina HiSeqs2500, paired-end. Data is described as follows:
Sample ID – sequencing depth, length of reads. Quantity of reads remaining after

data processing, described in supplementary information.
Malaria Maf fl/fl:
GAN719A3- 355024714(x2) reads, length 51 nt. Quality control and processing resulted in 173310313 reads.
GAN719A21- 312476181(x2) reads, length 51 nt. Quality control and processing resulted in 147589106 reads.
GAN719A22- 322625689 (x2) reads, length 51 nt. Quality control and processing resulted in 134514415 reads.

Malaria Maf fl/fl CD4Cre:
GAN719A4- 350641802 (x2) reads, length 51 nt. Quality control and processing resulted in 134514415 reads.
GAN719A11- 355324979 (x2) reads, length 51 nt. Quality control and processing resulted in 147486992 reads.
GAN719A12- 356720441 (x2) reads, length 51 nt. Quality control and processing resulted in 147402576 reads.

HDM allergy Maf fl/fl:
GAN719A5- 342362988 (x2) reads, length 51 nt. Quality control and processing resulted in 147402576 reads.
GAN719A15- 345626232 (x2) reads, length 101 nt. Quality control and processing resulted in 175866057 reads.
GAN719A17- 309429135 (x2) reads, length 51nt. Quality control and processing resulted in 134272611 reads.

HDM allergy Maf fl/fl CD4 Cre:
GAN719A6- 356793270 (x2) reads, length 51 nt. Quality control and processing resulted in 153200843 reads.
GAN719A18- 327015288 (x2) reads, length 51 nt. Quality control and processing resulted in 123984864 reads.
GAN719A27- 180711873 (x2) reads, length 101 nt. Quality control and processing resulted in 97866988 reads.

EAE Maf fl/fl:
GAN719A20- 171209809 (x2) reads, length 51 nt. Quality control and processing resulted in 40686167 reads.
GAN719A24- 178313808 (x2) reads, length 101 nt. Quality control and processing resulted in 45610741 reads.
GAN719A26- 186452585 (x2) reads, length 101 nt. Quality control and processing resulted in 51441647 reads.

EAE Maf fl/flCD4 Cre:
GAN719A19- 167390937 (x2) reads, length 51 nt. Quality control and processing resulted in 39080438 reads.
GAN719A23- 171694244 (x2) reads, length 101 nt. Quality control and processing resulted in 39847852 reads.
GAN719A25- 189463614 (x2) reads. Length 101 nt. Quality control and processing resulted in 50105695 reads.

7. Describe the antibodies used for the ChIP-seq experiments.

Illumina Nextera kit Cat #FC-121-1030 was used to generate libraries, amplified for 11 cycles with Nextera PCR Primers.

8. Describe the peak calling parameters.

MACS2 2.1.1 software was used to call peaks with the following parameters:
--keep-dup all: do not remove duplicated alignment (already removed using Picard software)
--nomodel --shift -100 --extsize 200: selected according to software documentation to look for enrichment of insertion sites (Tn5 transposase)
selected all peaks with q-value < 0.01 (default parameter)
A consensus peak set was retrieved per disease model (called with a q-value < 0.01). Due to the minimal changes in accessibility, peaks called irrespective of their genotype were considered. The quantities of peaks analysed go as follows: malaria: 87533, HDM: 54745, EAE: 42286 peaks. See also supplementary information.

9. Describe the methods used to ensure data quality.

FastQC_0.11.5: for overall quality assessment
Skewer 0.2.2: sequencing quality control
IGV_2.3.97: genome browser visual inspection of ATAC-seq peaks in BED format
SAMtools 1.3.1 for alignment QC (discarded alignments with a mapQ < 30)

MACS2 2.1.1 software was used to call peaks with the following parameters:
--keep-dup all: do not remove duplicated alignment (already removed using Picard software)
--nomodel --shift -100 --extsize 200: selected according to software documentation to look for enrichment of insertion sites (Tn5 transposase)
selected all peaks with q-value < 0.01 (default parameter)
A consensus peak set was retrieved per disease model (called with a q-value < 0.01). Due to the minimal changes in accessibility, peaks called irrespective of their genotype were considered. The quantities of peaks analysed go as follows: malaria: 87533, HDM: 54745, EAE: 42286 peaks. See also supplementary information.

10. Describe the software used to collect and analyze the ChIP-seq data.

FastQC_0.11.5: for overall quality assessment
BWA-MEM: map pair-end reads to mm10
BEDTools 2.26.0: convert alignments from bam to bed format
Awk: command line tool. Used to remove alignments done to mitochondrial DNA, shift reads in the forward strand by + 4bp or reverse strand by -5 bp , and to remove fragments with a size >99bp.
MACS2 2.1.1: peak-calling
Diffbind 2.0.2: peak read quantification to test for differential changes in chromatin accessibility.
BaGFoot: test for differential TF activity based on changes in Tn5 insertions on motif matching sites.
DeepTools 2.4.2: bamCoverage command to retrieve RPKM normalised
IGV_2.3.97: genome browser visual inspection of ATAC-seq peaks in BED format
R statistical software for data integration and visualization.
See also supplementary information.

nature research

Corresponding author(s): Dr. Anne O'Garra

ChIP-seq Reporting Summary

Form fields will expand as needed. Please do not leave fields blank.

Data deposition

1. For all ChIP-seq data:

☐ a. Confirm that both raw and final processed data have been deposited in a public database such as GEO.

☐ b. Confirm that you have deposited or provided access to graph files (e.g. BED files) for the called peaks.

2. Provide all relevant data deposition access links. *The entry may remain private before publication.*	Not applicable, a previously published c-Maf ChIP-seq dataset, Ciofani et al. Cell (2012) (GEO ID: GSE40918) was used.
3. Provide a list of all files available in the database submission.	Not applicable, a previously published c-Maf ChIP-seq dataset, Ciofani et al. Cell (2012) (GEO ID: GSE40918) was used.
4. Provide a link to an anonymized genome browser session (e.g. UCSC), if available.	Not applicable, a previously published c-Maf ChIP-seq dataset, Ciofani et al. Cell (2012) (GEO ID: GSE40918) was used.

Methodological details

5. Describe the experimental replicates.	In our study, we used a previously published c-Maf ChIP-seq dataset, Ciofani et al. Cell (2012) (GEO ID: GSE40918). The two available replicates for c-Maf ChIP-seq (SRA IDs: SRR571559, SRR571560) and one input sample (SRR571773) were analysed.
6. Describe the sequencing depth for each experiment.	All ChIP-seq sequencing reads were single-ended. Sample ID – sequencing depth, length of reads. Quantity of reads remaining after data processing, described in supplementary information. SRR571559 (c-Maf ChIP_1): 52162677 reads, length 36 nt., 31791915 mapped reads SRR571560(c-Maf ChIP_2): 37065021 reads, length 36 nt., 15665482 mapped reads SRR571773 (input): 45350912 reads, length 36 nt., 30722515 mapped reads
7. Describe the antibodies used for the ChIP-seq experiments.	Not Applicable. Used publicly available GEO dataset: GSE40918
8. Describe the peak calling parameters.	MACS2 2.1.1 software was used to call peaks with the following parameters: default parameters, suitable for ChIP-seq analysis. Selected all peaks with q-value < 0.01 (default parameter). For each replicate, peaks were called individually and used the same ChIP input sample for both. See also supplementary information.
9. Describe the methods used to ensure data quality.	FastQC_0.11.5: for overall quality assessment IGV_2.3.97: genome browser visual inspection of ChIP-seq peaks in BED format MACS2 2.1.1 software was used to call peaks with the following parameters: default parameters, suitable for ChIP-seq analysis. Selected all peaks with q-value < 0.01 (default parameter). For each replicate, peaks were called individually and used the same ChIP input sample for both. See also supplementary information. A consensus peak set was generated from the union of both replicates (peaks with a q-value <0.01). For overlapping peaks between replicates, the one with the highest confidence score was kept. This resulted in 45,727 c-Maf ChIP-seq peaks. See also supplementary information.
10. Describe the software used to collect and analyze	Trimmomatic 0.36: sequencing quality based trimming (parameters HEADCROP:2

10. Describe the software used to collect and analyze the ChIP-seq data.

TRAILING:25 MINLEN:26)
Bowtie 1.1.2: map single-end reads (parameters y -m2 --best --strata -S)
BEDTools 2.26.0: convert alignments from bam to bed format
MACS2 2.1.1: peak-calling
IGV_2.3.97: genome browser visual inspection of ChIP-seq peaks in BED format
R statistical software for data integration and visualization.
See also supplementary information.